International Journal of Extreme Manufacturing

Recent advances in fabricating high-performance triboelectric nanogenerators via modulating surface charge density

Zekun Li, Aifang Yu, Qing Zhang, Junyi Zhai

View online: https://doi.org/10.1088/2631-7990/ad4f32

International Journal of Extreme Manufacturing

Recent advances in fabricating high-performance triboelectric nanogenerators via modulating surface charge density

OPEN ACCESS
IOP Publishing | IMMT
International Journal of Extreme Manufacturing
Int. J. Extrem. Manuf. **6** (2024) 052003 (22pp)
https://doi.org/10.1088/2631-7990/ad4f32

Topical Review

Recent advances in fabricating high-performance triboelectric nanogenerators via modulating surface charge density

Zekun Li[1,2,4], **Aifang Yu**[1,2,4], **Qing Zhang**[3,*] **and Junyi Zhai**[1,2,*]

[1] Beijing Key Laboratory of Micro-Nano Energy and Sensor, Center for High-Entropy Energy and Systems, Beijing Institute of Nanoenergy and Nanosystems, Chinese Academy of Sciences, Beijing 101400, People's Republic of China
[2] School of Nanoscience and Engineering, University of Chinese Academy of Sciences, Beijing 100049, People's Republic of China
[3] Center for Micro- and Nano-Electronics, School of Electrical and Electronic Engineering, Nanyang Technological University, Singapore 639798, Singapore

E-mail: qzhang@ntu.edu.sg and jyzhai@binn.cas.cn

Received 11 February 2024, revised 28 March 2024
Accepted for publication 21 May 2024
Published 12 June 2024

Abstract

Triboelectric nanogenerators (TENGs), a type of promising micro/nano energy source, have been arousing tremendous research interest since their inception and have been the subject of many striking developments, including defining the fundamental physical mechanisms, expanding applications in mechanical to electric power conversion and self-powered sensors, etc. TENGs with a superior surface charge density at the interfaces of the electrodes and dielectrics are found to be crucial to the enhancement of the performance of the devices. Here, an overview of recent advances, including material optimization, circuit design, and strategy conjunction, in developing TENGs through surface charge enhancement is presented. In these topics, different strategies are retrospected in terms of charge transport and trapping mechanisms, technical merits, and limitations. Additionally, the current challenges in high-performance TENG research and the perspectives in this field are discussed.

Keywords: triboelectric nanogenerators, surface charge density, material optimization, circuit design

[4] These authors contributed equally.
[*] Authors to whom any correspondence should be addressed.

2631-7990/24/052003+22$33.00

1. Introduction

Fossil fuels (e.g. coal, gas, and fossil oil), which are widely available, highly energy-dense, and easily extracted, have been utilized to convert their chemical energy into electric energy through steam or combustion engines for centuries. However, excessive demand for fossil fuels has led to significant greenhouse gas emissions, exacerbating global climate change and pollution. Meanwhile, traditional fossil fuels are being depleted, creating an energy crisis for human society [1–10]. In that regard, it has become more urgent than ever to develop cutting-edge energy technologies to mitigate dependence on the conventional energy sources, ease the burden on the environment, and provide low-carbon electricity for the future. Triboelectric nanogenerators (TENGs) invented by Z L Wang's group offer a revolutionary alternative to traditional sources of energy [11]. With TENGs, any form of irregular and randomly distributed mechanical energy (e.g. wind, wave, vibrations, human motions, vehicle movement, etc) can be harvested and converted into electricity. Particularly suited to powering thousands of randomly dispersed sensor nodes of all types and sizes, TENGs are lightweight, easy to manufacture, and cost-effective, as opposed to chemical batteries. Currently, TENG has become a research hotspot across multiple disciplines, demonstrating up-and-coming applications in self-charging packages [12–15], self-powered systems [16–19], high-voltage sources [20], medical electronics that are wearable or implantable [21–25], human-machine interfaces [26–29], artificial intelligence [30, 31], smart agriculture [32, 33], marine ranching [34], smart cities [35], blue energy [36–40] and more. It is estimated that there are over 12 000 scientists engaged in nanogenerators from 83 countries and regions worldwide [41].

How to efficaciously boost the electrode surface charge density of TENGs to achieve high power TENGs is crucial for the future commercial application of TENGs [13]. For TENG research in its early stage, the common methods used to enhance the output performance are the exploration of novel device structures and material surface engineering [42–55]. Novel materials and combinations of materials with different features are being explored for the preparation of outstanding performance TENGs. To overcome the air breakdown effect and determine the TENG charge density limit, recent proposals suggest implementing environmental control, ion irradiation, and circuit-related strategies to manufacture high-output TENGs and achieve breakthroughs in their surface charge density [56–61]. As of today, TENGs are able to generate 98.72 mC m^{-2} of charge density and 10 MW m^{-2} of peak power density [62, 63]. The fast development of high-output TENG deserves a retrospection of the recent progress in boosting the electrode surface charge density. On the one hand, it can provide researchers with a blueprint and reference to the current fabrication of high charge density TENGs. On the other hand, it can also serve as a guide for researchers who are fresh to the field of TENG.

Here, a retrospection of recent advances in high surface charge density TENG covers from the perspectives of material optimization, external circuit design, and strategy conjunction, as shown in figure 1. As a matter of triboelectric material optimization, our main focus is on bulk modification of the materials, which offers the benefits of a variety of materials, flexible modification methods, and substantial performance improvements. Modifying the bulk phase of triboelectric materials is primarily concerned with improving their capacity to store charges, including dielectric constant control, charge storage enhancement, and leakage charge minimization. In external circuit design, self-charge excitation (SCE), external charge pumping (ECP), and external charge excitation are the focus since they offer huge performance gains and are easy to integrate. Further, this review also discusses the synergistic strategies of material optimization in tandem with circuit design, as their interplay can yield a higher surface charge density than employing either enhancement strategy in isolation. Additionally, we also highlight some areas that require further improvement in current high-performance TENG research, including charge storage mechanism, performance test criteria, application exploration, and effective power management and storage.

2. Material optimization

The electrode surface charge density is one of the key performance indicators as it determines the transferred charge, induced current, voltage, and output power of TENGs [73]. The surface charge density can be regarded as the overall charge density on the dielectric (or on the electrode) whose sources include: triboelectric charge from contact electrification, depositing charges through corona charging (or air ionization gun) and charge exchanged with external circuits [71]. From a material perspective, the capability of friction polymer to produce and store triboelectric charges determines the surface charge density. Early research efforts therefore focused on surface engineering of dielectrics to enhance the ability of the materials to generate triboelectric charges. However, contact separation (or sliding friction) unfortunately results in surface engineering failures due to wear and tear of the material surfaces [63]. Further, the relatively complex manufacturing process of surface engineering would make it difficult to manufacture surface-modified materials on a large scale [42–44]. Consequently, bulk phase modification of dielectric materials with enhanced triboelectric charge storage capabilities has received increasing attention in recent years. Two kinds of bulk phase modifications for triboelectric materials are efficient: one is to amplify their dielectric constant, and the other is to strengthen their ability to trap triboelectric charge.

2.1. Dielectric constant control

It has been found that amplifying the permittivity of the triboelectric dielectric material results in enhancement in the

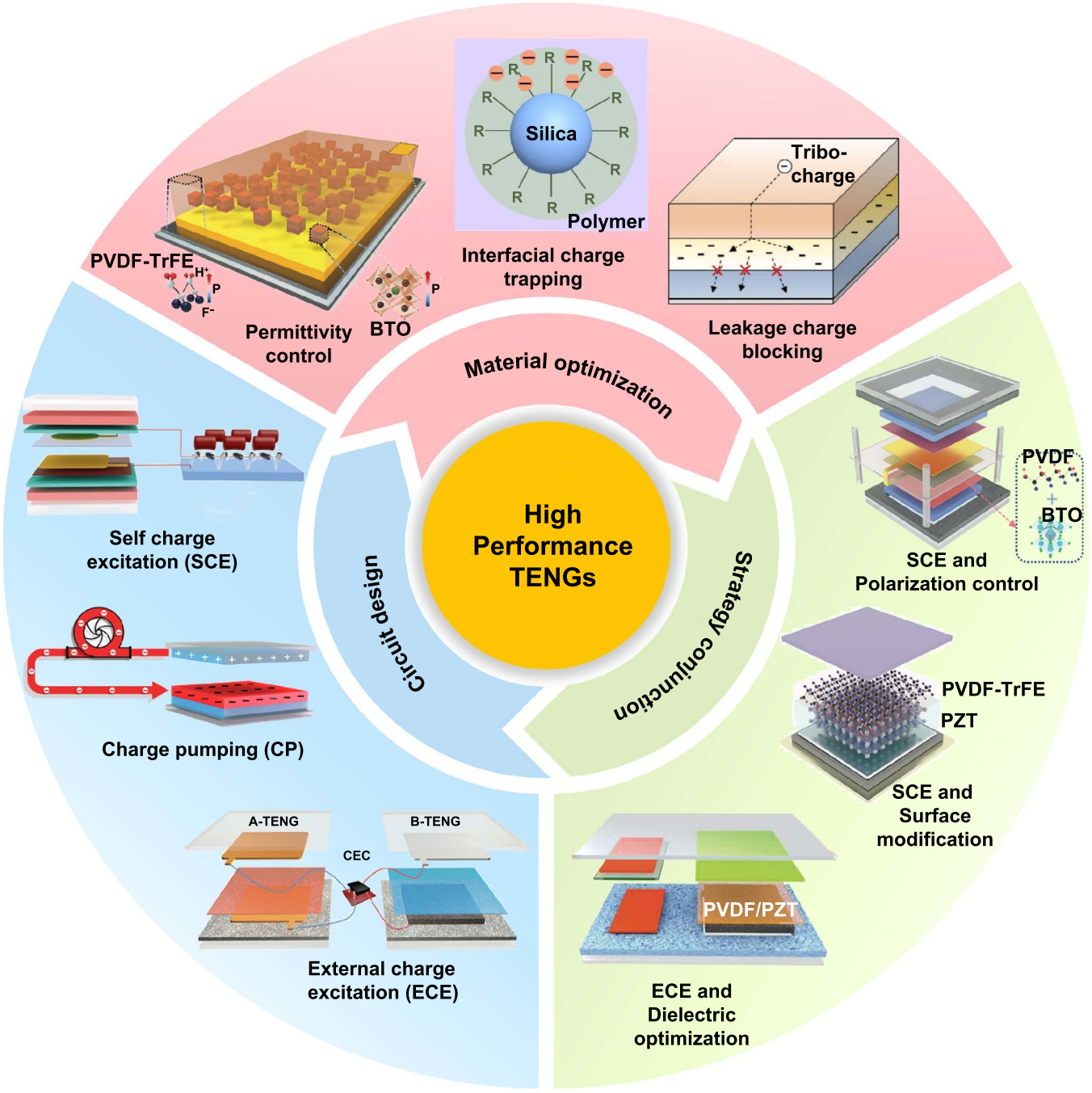

Figure 1. A blueprint of the recent advances in the manufacture of high-performance TENGs. Strategy conjunction: [64] John Wiley & Sons. © 2022 Wiley-VCH GmbH. [65] John Wiley & Sons. © 2022 Wiley-VCH GmbH. [66] John Wiley & Sons. © 2023 Wiley-VCH GmbH. Circuit design: [67] John Wiley & Sons. © 2021 Wiley-VCH GmbH. [68] John Wiley & Sons. © 2022 Wiley-VCH GmbH. Reprinted from [69], © 2018 Elsevier Ltd All rights reserved. Material optimization: [70] John Wiley & Sons. © 2016 WILEY-VCH Verlag GmbH & Co. KGaA, Weinheim. [71] John Wiley & Sons. © 2021 Wiley-VCH GmbH. Reproduced from [72],Copyright © 2023, Tsinghua University Press.

triboelectric charge, as the triboelectric dielectric layer is considered a part of a parallel plate capacitor [74–78]. In this case, incorporating high dielectric constant nanoparticles into the polymer to amplify the material's dielectric constant is a promising approach to boost the output. For example, $BaTiO_3$ (BTO) is the most commonly used high permittivity filler and it has been reported to increase the dielectric constant of poly(vinylidenefluoride-co-trifluoroethylene) (PVDF-TrFE) [70], as depicted in figure 2(a). It is seen that the TENG output increases initially, but then decreases as

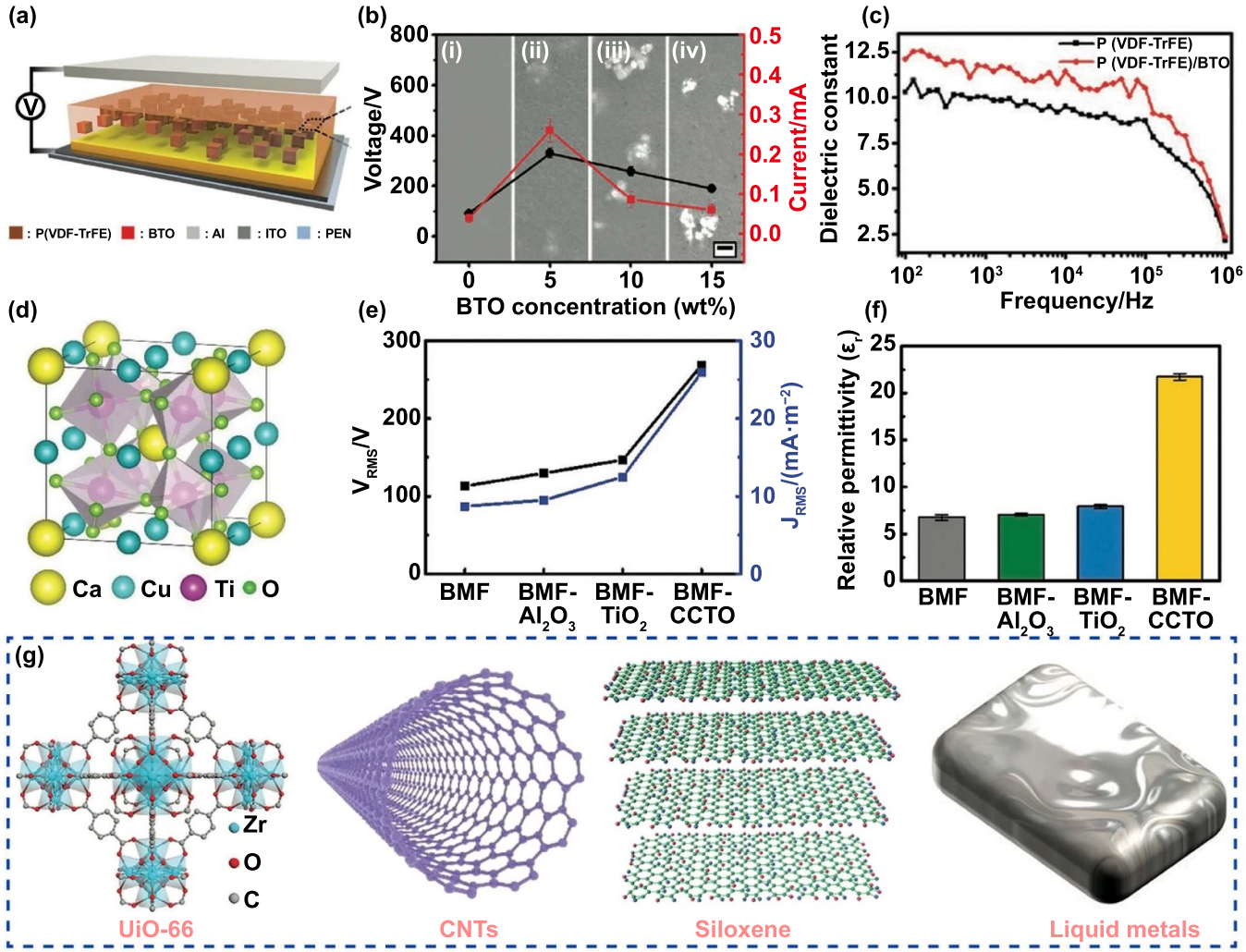

Figure 2. Modulation of the dielectric constant of triboelectric materials by doping nanomaterials. (a) A TENG prepared from PVDF-TrFE/BTO composite. (b) Performance of composites with different BTO concentrations. (c) Dielectric constant of PVDF-TrFE/BTO composite film. (a)–(c) [70] John Wiley & Sons. © 2016 WILEY-VCH Verlag GmbH & Co. KGaA, Weinheim. (d) Crystal structure of CCTO. (e) Dielectric constant of BMF composite film doped with different nanoparticles. (f) Output performance of BMF composite film doped with different nanoparticles. (d)–(f) [79] John Wiley & Sons. © 2020 WILEY-VCH Verlag GmbH & Co. KGaA, Weinheim. (g) Selection of materials used to enhance the dielectric constant of friction materials. [80] John Wiley & Sons. © 2021 Wiley-VCH GmbH. [81] John Wiley & Sons. © 2023 Wiley-VCH GmbH. [82] John Wiley & Sons. © 2022 Wiley-VCH GmbH. [83] John Wiley & Sons. © 2023 Wiley-VCH GmbH.s

the particle concentration increases to 15 wt%, as presented in figure 2(b). TENG based on PVDF-TrFE/BTO composite outputs a current of 0.3 mA and a voltage of 300 V when BTO concentration is 5 wt%, which is six times and three times greater than PVDF-TrFE. The reason for the improved output can be attributed to the fact that the composite film possesses a larger dielectric constant than the PVDF-TrFE film as presented in figure 2(c). As a consequence of the profusion of BTO particles appearing on the composite surface (figure 2(b-iii)), the film becomes less capable of attracting electrons, resulting in a deterioration of the output performance.

In Maxwell's model, as well as the amount of nanofillers in the composite dielectric, the permittivity of the nanofillers themselves affects the permittivity of the composite and hence TENG performance [71]. Accordingly, $CaCu_3Ti_4O_{12}$ (CCTO), a filler with a giant dielectric constant of 7500, was introduced into butylated melamine formaldehyde (BMF) to strengthen the generating capacity of the material and compared with BMF reinforced by fillers with different dielectric constants (Al_2O_3 and TiO_2) [79], as depicted in figures 2(d) and (e). As a consequence, it has been shown that fillers with a high permittivity can significantly increase the relative permittivity of BMF (figure 2(f)), thereby upgrading TENG performance. Besides employing high-k materials as fillers, as shown in figure 2(g), novel materials have also been exploited as fillers, including Metal-Organic Frameworks (UiO-66) [80], one-dimensional materials (carbon nanotubes (CNTs), silver nanowires) [81, 84], two-dimensional materials (Slioxene,

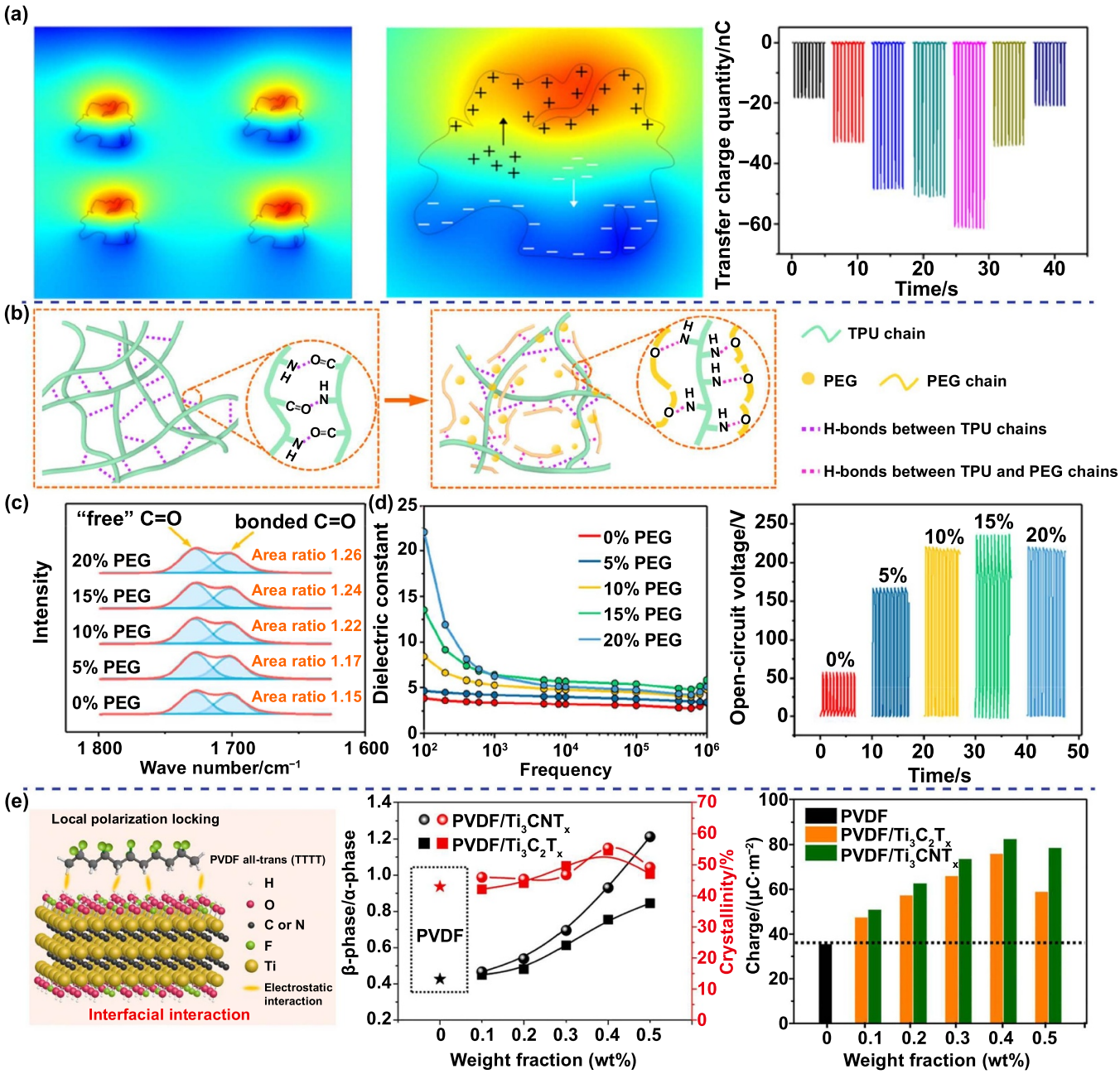

Figure 3. Incorporating modifiers into triboelectric materials to regulate their polarization. (a) Simulation of interfacial polarization and output charge of PVDF/AC composite films. (a) Reprinted with permission from [86]. Copyright (2020) American Chemical Society. (b)–(d) Molecular structure, FTIR, dielectric constant, and output of TPU/PEG composite films. (b)–(d) Reprinted with permission from [87]. Copyright (2021) American Chemical Society. (e) Interface polarization, polar phase content, and output performance of PVDF/MXene composite films. (e) Reprinted from [85], © 2021 Elsevier Ltd All rights reserved.

MXene) [82, 85], and even liquid metals [83], demonstrating the diversity of materials that can be utilized to upgrade the permittivity of polymers.

Amplifying the permittivity of triboelectric materials can also be accomplished by manipulating the polarization at the interface region between the particle and polymer from a micro- to nanoscale. As shown in figure 3(a), Jin and co-workers modified the polyvinylidene fluoride (PVDF) thin film using active carbon (AC) particles with high specific surface areas and simulated charge distribution at the particle polymer interface using COMSOL Multiphysics [86]. There are plentiful interfaces within the PVDF/AC composite that can be polarized by an external electric field, which leads to a refinement of the permittivity of the PVDF/AC composite in comparison to the PVDF. It is worthwhile to note, however, that when the AC particle content in the composite

film exceeds a certain level, particles agglomerate, resulting in fewer interfaces that are polarizable, which subsequently diminishes the dielectric constant of the film. Thus, TENGs based on composite films experience an initial improvement and then a decline in transferred charge with increasing AC particle concentration.

Understanding interfacial polarization in terms of changes in the composition of the filler and dielectric at the interface is another methodology. The thermoplastic polyurethane (TPU) chain typically contains a substantial number of hydrogen bonds between the N-H groups and the carbonyl groups as well as between the N-H groups and the ester carbonyl groups [87], as illustrated in figure 3(b). Polyethylene glycol (PEG) added to the TPU matrix will form stronger hydrogen bonds with the N-H group of the TPU chain, resulting in the breakdown of hydrogen bonds within the TPU. This thus theoretically strengthens the polarization capacity of TPU chains and increases the free C=O content of TPU/PEG composites. The Fourier Transform Infrared Spectroscopy (FTIR) of the composite film in figure 3(c) demonstrates that as expected, the free C=O to fixed C=O peak area ratio increased from 1.15 to 1.26 when the PEG concentration was upgraded. A further evaluation of the composites' permittivity and generating capacity is demonstrated in figure 3(d), where the permittivity of the TPU/PEG increases from 3.85 to 22.02 (PEG concentration: 20%, frequency: 100 Hz). Accordingly, open-circuit voltages of the composite films increase and then decline with improving PEG content, which is due to excessive PEG doping causing dielectric breakdown during corona charging. As portrayed in figure 3(e), it is also possible to manipulate the chemical structure of the interface between the filler and polymer by adding two-dimensional materials ($T_3C_2T_x$ or Ti_3CNT_x) with different surface termination groups [85]. As a consequence, the ratio of β-phase/α-phase in polymer matrix increases from 0.44 to 0.84 in the PVDF/$T_3C_2T_x$ (1.21 for the PVDF/Ti_3CNT_x) when the concentration of 2D fillers is 0.5 wt%. Since the β-phase is more polar, the permittivity of the PVDF/$T_3C_2T_x$ (PVDF/Ti_3CNT_x) composite is enhanced, which results in a higher charge density.

2.2. Charge trapping

The dynamic balance between generation and annihilation of triboelectric charges during TENG operation determines its output performance. Recent research has shown that by strengthening the charge trap capacity of the material, the leakage and escape charge can be significantly lessened, thereby improving TENG surface charge density. As of present, strategies that can enhance the charge-trapping capability of triboelectric materials can be categorized into two categories: one is the doping of fillers, and the other is the addition of a charge-blocking layer. The degree of energy band matching between the particle and the polymer should be considered when doping the charge trapping material, as this determines how the triboelectric charge is transferred to and trapped within the triboelectric polymer. Accordingly, $Cs_3Bi_2Br_9$ with high defect density was doped as a charge-trapping material into poly (vinylidene fluoride co hexafluoropropylene) (PVDF-HFP) nanofibers [88], as displayed in figure 4(a). In comparison to materials such as $MAPbBr_3$, $FAPbI_3$, rGO, ZnO, and MoS_2, there is an energy band difference of around 0.3 eV between $Cs_3Bi_2Br_9$ and PVDF-HFP, which facilitates charge transport. As portrayed in figure 4(b), when the concentration of $Cs_3Bi_2Br_9$ is improved from 0 to 1 wt%, the current of PVDF-HFP/$Cs_3Bi_2Br_9$ composite nanofibers is increased by approximately 118%. In the case of a $Cs_3Bi_2Br_9$ concentration greater than 2 wt%, excess $Cs_3Bi_2Br_9$ would emerge on the surface of composite nanofibers, forming a leaking channel for the captured charge and, as a consequence, the charge trapping performance of the PVDF-HFP/ $Cs_3Bi_2Br_9$ composites is limited.

Recently, it has been found that modulation of the interfacial functional groups between the particle and the triboelectric polymer can also raise the capability of the material to trap triboelectric charges. As presented in figure 4(c), silica nanoparticles (SNPs) modified with perfluorosilane coupling agents were doped into PVDF to change the interface between PVDF and fillers and make it better at capturing charge [72]. The transferred charge density (TCD) based on the composite film TENG improves with increasing chain length of the interfacial functional groups, as demonstrated in figure 4(d). Further, the decay of TCD with time reveals the different charge storage capacities of the interfacial functional groups. After the same decay time (420 s), the TCD of PVDF film was 6.5 μC m^{-2}, while that of PVDF/ PFD-SNPs was 40 μC m^{-2} (23 μC m^{-2} for PVDF/PFH-SNPs and 35 μC m^{-2} for PVDF/PFO-SNPs). It can be seen that raising the chain length of the interfacial functional group results in a higher charge trapping capacity of the interface. As triboelectric materials become more capable of capturing and storing triboelectric charges, their output performances are found to be enhanced in both regular and high humidity environments. As demonstrated in figure 4(e), water-absorbent HKUST-1 was employed to enhance the charge trap capacity and triboelectric output of polydimethylsiloxane (PDMS) in high humidity conditions [89]. It was found that the short-circuit current of pure PDMS decreased as the relative humidity (RH) improved, just as it does in normal TENGs. However, the current of PDMS/HKUST-1 (5 wt%) improved with the rise of RH, as shown in figure 4(f). Further charge decay experiments revealed that the charge decay time of pure PDMS-based TENG declines with increasing RH (from 10% to 90%). In contrast, the decay time of PDMS/HKUST-1 (5 wt%)-based TENG showed the inverse tendency, increasing from 500 min to 1200 min, as demonstrated in figure 4(g). The results of these experiments indicate that HKUST-1 enhances the triboelectric charge capture capability and storage depth of PDMS at different humidity levels, thereby improving the output of the TENG in a high RH environment.

Employing charge trap materials between the attached electrode and the friction material is another technique to intensify the trapping of frictional charge by the dielectric. Polystyrene (PS) was first proposed by Cui *et al* [90] to strengthen the triboelectric charge storage capacity of PVDF. It has been recently reported that PDMS has a higher trap density than PS, which can further enhance the charge storage capacity of PVDF [91].

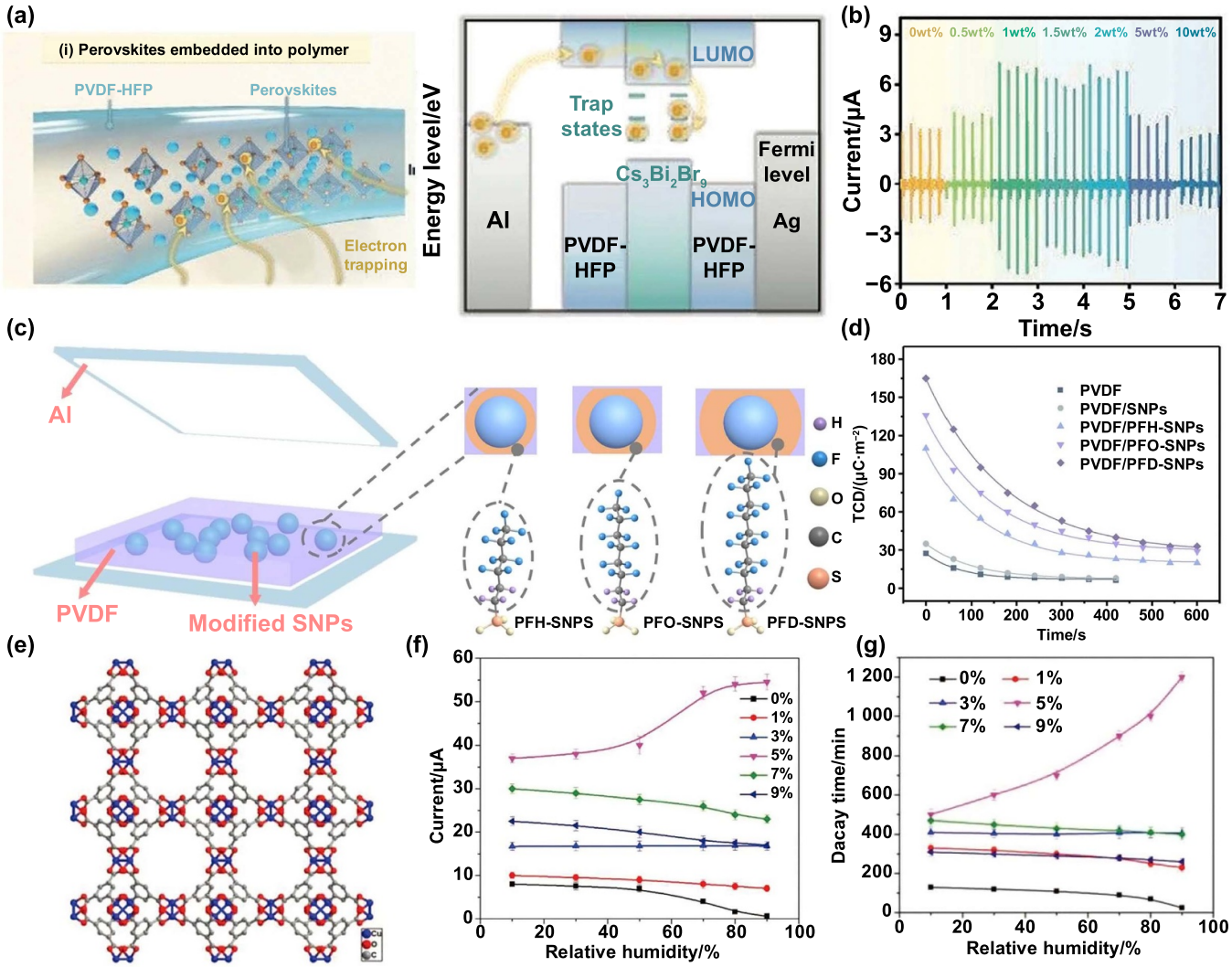

Figure 4. Strengthening the charge capture capacity of triboelectric polymers with nanoparticles. (a) Energy bands of PVDF-HFP/$Cs_3Bi_2Br_9$ composite. (b) Output performance of PVDF-HFP/$Cs_3Bi_2Br_9$ composite. (a)–(b) [88] John Wiley & Sons. © 2022 Wiley-VCH GmbH. (c) Different interfaces in PVDF/modified SNPs composite films. (d) The output performance of PVDF/modified SNPs composites. (c)–(d) Reproduced from [72], Copyright © 2023, Tsinghua University Press. (e) The structure of HKUST-1. (f) Current of the PDMS/HKUST-1 composite at varying RH. (g) Charge decay time of the PDMS/HKUST-1 composite at varying RH. (e)–(g) [89] John Wiley & Sons. © 2019 WILEY-VCH Verlag GmbH & Co. KGaA, Weinheim.

As shown in figure 5(a), the difference in Fermi levels between PVDF and Al results in charge transfer from Al to PVDF when PVDF and Al come into contact. Subsequently, the induced electric field causes the charges captured in the shallow traps in the PVDF to be neutralized by the opposite charges on the attached Al, causing output degradation. By incorporating PDMS as a charge trap layer, the triboelectric charge is further captured by its deep traps, resulting in a boost in the output. When PDMS reaches a certain thickness, electrostatic induction is weakened, resulting in a reduction in performance.

The triboelectric film thickness also affects the charge capture. A TENG with perfluoroalkoxyalkane (PFA) as the negative charge generation layer, molybdenum sulfide (MoS_2) as a positive charge generation layer and SiO_2 as a charge capture material was constructed to investigate the triboelectric layer thickness on the performance [92]. Figure 5(b) displays that the triboelectric pair composed of SiO_2 and PFA produces an output of 107.8 μC m^{-2}. With the increasing thickness of the MoS_2 coated on the SiO_2 layer, TENG's charge density increases initially, but then decreases. When MoS_2 thickness is 50 nm, the optimal output of TENG exceeds 1000 μC m^{-2}. According to the simulation results of the triboelectric electric field strength as the friction layer thickness is varied, the positive charges that are formed on the MoS_2 layer can be transported to the interface with the SiO_2 layer within a specified thickness range. After the positive charge is transferred to the region between the MoS_2 and the SiO_2, the surface of MoS_2 becomes electrically neutral, thus further increasing the charge generation by facilitating charge transfer between MoS_2 and PFA. If the thickness of the MoS_2 covering the SiO_2 exceeds a certain value, the work function of the MoS_2 increases. This results in a decrease in the amount of charge transferred to the positive friction layer during the contact process, leading to a decline in the TENG's charge density. It should be noted that

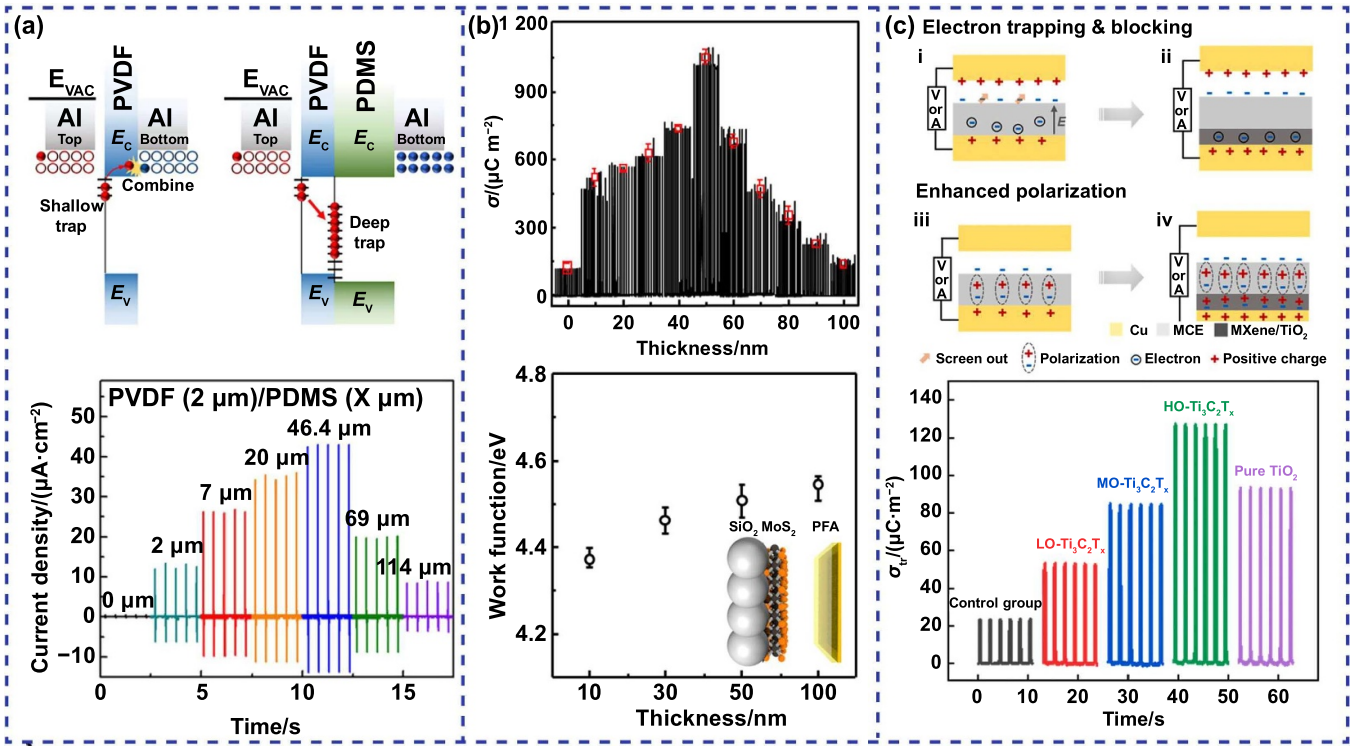

Figure 5. Enhancing triboelectric output by introducing charge blocking layers. (a) Band diagram and output performance of PVDF/PDMS composite films. (a) Reprinted from [91], © 2018 Elsevier Ltd All rights reserved. (b) The influence of MoS_2 thickness on the charge density of the MoS_2/SiO_2 composite layer and the electric field distribution of the MoS_2/SiO_2 composite layer. (b) Reproduced from [92] with permission from the Royal Society of Chemistry. (c) Output enhancement mechanism and charge density of MCE/MXene/TiO_2 composite materials. (c) Reprinted from [93], © 2022 Elsevier Ltd All rights reserved.

the interlayer can be used not only as a charge capture layer but also as a polarization material to amplify the permittivity of the dielectric [93]. The triboelectric performance of mixed cell esters (MCE) thin film was upgraded using MXene/TiO_2 composite capable of both charge capture and dielectric constant enhancement, as portrayed in figure 5(c). Changing the degree of oxidation of MXene (or the amount of TiO_2 contained in the MXene layer) could easily regulate the output of the MCE/MXene/TiO_2 composite. The charge density of the MCE/MXene/TiO_2 composite increased from 23.8 μC m^{-2} to 128 μC m^{-2} as the oxidation of the MXene film increased. Comparatively, 94 μC m^{-2} of charge density is obtained by TENG when TiO_2 is utilized as an interlayer, further indicating that MXene/TiO_2 composites can improve the performance of the MCE through the conjunction of charge capture and polarization enhancement. A comparison of common triboelectric materials under different filler reinforcements is provided in table 1.

3. Circuit design

Although material modification has made significant progress in boosting the surface charge density, the drift and diffusion of triboelectric charges, thermal emission, and air breakdown effects have hindered further improvement of surface charge density [111]. Diverse advanced technologies have been proposed for achieving ultra-high surface charge density, including environmental control, corona charging, charge pumping (CP), and charge excitation (CE) [56–61]. Among them, CP and CE are experiencing rapid development due to their advantages such as simplicity of structure, broad applicability, excellent compatibility, and ultra-high output. By utilizing circuitry, CP and CE directly boost the surface charge density on the TENG's electrode, whereas in conventional TENG, the output charge is commonly restricted by the finite charge bound on the triboelectric polymer. It is the purpose of this section to briefly introduce the device structure, circuit composition, working mechanism, and recent progress of SCE-TENG, ECP-TENG, and external charge excitation (ECE-TENG).

3.1. ECP

The concept of CP was first proposed by Xu and co-workers in their construction of the ECP-TENG [69]. Typically, ECP-TENG is divided into three components, as displayed in figure 6(a): a pump TENG (p-TENG) serves as the charge provider, a main TENG (m-TENG) serves to output charge, and a full-wave rectifier bridge. Whenever a vertical force is implemented, the dielectric and the metal layer of the m-TENG will first come into contact, forming a parallel plate capacitor as the

Table 1. A comparison of triboelectric materials under various filler reinforcements.

Polymer matrix	Filler	Counter layer	Current/charge density	Dielectric constant	Durability	References
PVDF	Hydrophobic SiO_2	PHBV	20 mA m^{-2}	—	—	[94]
	PDMS/BT	PHBV	13 mA m^{-2}, 58 μC m^{-2}	4	—	[95]
	Printer ink	Cu	150 mA m^{-2}	—	1000	[96]
	Co-NPC	Nylon 11	210 mA m^{-2}, 392 μC m^{-2}	22	60 000	[97]
	$BaTiO_3$	Rubber	19.02 mA m^{-2}, 105.6 μC m^{-2}	—	—	[98]
	ZnAl-LDH	PET	56 mA m^{-2}	38.9		[99]
	Graphene	PA6	189 mA m^{-2}, 352 μC m^{-2}	—	80 000	[100]
	Ti_3CNT_x	Cu	20.1 mA m^{-2}, 82 μC m^{-2}	19	100 000	[85]
PDMS	$NaNbO_3$	Al	23 mA m^{-2}, 68 μC m^{-2}	3.3	90 000	[101]
	$BaTiO_3$	Nylon	50 μC m^{-2}	67	10 000	[102]
	Graphene oxide	Skin	5.11 μC m^{-2}	—	14 400	[103]
	$SrTiO_3$	Cu	190 μC m^{-2}	—	15 000	[104]
	SWCNTs	Teflon	4.2 mA m^{-2}	280	20 000	[105]
PI	BNNS	Al	43 μC m^{-2}	4.2	1000	[106]
	MoS_2	Al	533 μC m^{-2}	—	—	[107]
Silicone	Co-NPC	Skin	98.5 mA m^{-2}, 11.4 μC m^{-2}	5	—	[108]
	MXene	Skin	200 mA m^{-2}	—	86 000	[109]
	Siloxene	Nitrile	50 mA m^{-2}	8	—	[82]
PVDF-HFP	$Cs_3Bi_2Br_9$	Al	16.3 mA m^{-2}	—	—	[88]
	Liquid metal	Al	150 μC m^2	3	14 400	[110]
TPU	PEG	PTFE	25 mA m^{-2}, 50 μC m^{-2}	8	10 000	[87]

m-TENG is easily compressible in comparison of p-TENG. When the vertical force is withdrawn, the p-TENG separates first. Note that the m-TENG maintains a contact state during the movement of the p-TENG, thus constantly accumulating charges from the external p-TENG. The above output mechanism was verified by further measurements of the pump charge Q_1 and the output charge Q_2. The output characteristics of Q_1 monotonically increase with time, while Q_2 has output characteristics of the normal TENG, and Q_2 upper limit overlaps well with Q_1. With this device configuration, the output of SCP-TENG can reach 1020 μC m^{-2} under atmospheric conditions, demonstrating the vigorous ability of the CP strategy to enhance TENG output.

The structure of ECP-TENG devices and their output modes have been further surveyed with the continuous development of CP. As presented in figure 6(b), the newly proposed ECP-TENG simplifies the device structure of the m-TENG and add a parallel capacitor [112]. During the movement of the p-TENG, carriers are accumulated in the buffer capacitor and the m-TENG (contact state) through a rectifier. Then, during the motion of the m-TENG, carriers can shuttle back and forth between m-TENG electrodes and capacitor electrodes in a symmetrical manner. ECP-TENG delivers a 1.5 mC m^{-2} output charge density since both the positive and negative sides can be used as output ports. There is also evidence that the two output ports can charge two 1 mF capacitors to 0.52 V and 0.54 V, respectively, which indicates that both ports are capable of charging or powering electronic devices. A CP strategy is also applied to rotation and sliding type TENG (RS-TENG), as well as the number of m-TENGs has been increased in pursuit of high output performance [113], as portrayed in figure 6(c). There is almost a linear increase in the charge and current of the RS-TENG with engaging more m-TENGs. Moreover, the as-fabricated RS-TENG can directly illuminate three 2 W bulbs, demonstrating its potential for use in self-powered systems.

3.2. External charge excitation

Meanwhile, external charge excitation (ECE) has also been utilized for high-performance TENGs. Figure 7(a) illustrates the scheme of an ECE-TENG, which mainly contains an excitation TENG (e-TENG), a voltage-multiplying circuit (VMC) with a Zener diode, and a m-TENG [114]. Note that a buffer layer composed of soft silicone, foam cushion, and liquid cushion is employed to achieve sufficient contact. ECE-TENG and ECP-TENG are similar in that both treat the exchange charge between the m-TENG and the circuit as the output. The differences between them include the fact that ECE-TENG can control surface charge density by adjusting the number of units in VMC and that the capacitors in VMC can directly serve as charge storage capacitors. Figure 7(b) shows that the effective charge density (ECD) of ECE-TENG increases almost linearly with the operation time before stabilizing at 0.72 mC m^{-2}. To further simplify the circuit composition and pursue higher output, two rectifier diodes and a capacitor consisting of a charge excitation circuit (CEC) and a soft carbon electrode were proposed to replace the VMC and copper electrodes of the initial ECE-TENG, respectively, as shown in figure 7(c). In an actual TENG device, the surface roughness of the metal electrode and polymer has a considerable influence on the contact efficiency of the electrode and dielectric, thus affecting the output of the device. There is an evidence that the employment of a

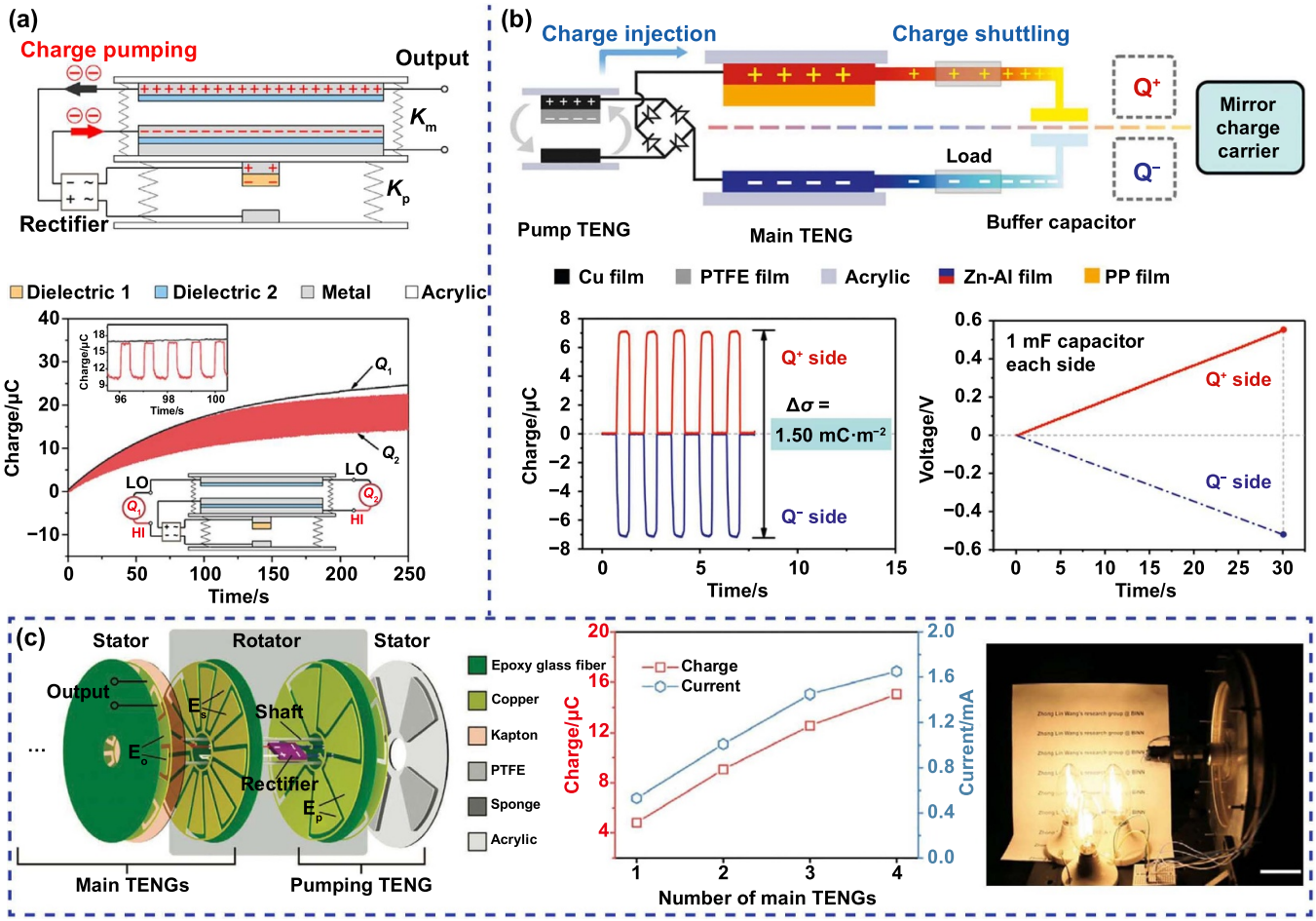

Figure 6. Charge pumping strategy for high-performance TENG. (a) The device configuration and the performance of the SCP-TENG. (a) Reprinted from [69], © 2018 Elsevier Ltd All rights reserved. (b) The device configuration and the output of the ECP-TENG. (b) Reproduced from [112]. CC BY 4.0. (c) The device configuration and the output of the RS-TENG. (c) [113] John Wiley & Sons. © 2020 WILEY-VCH Verlag GmbH & Co. KGaA, Weinheim.

flexible gel electrode can significantly improve the mechanical and electric contact properties of the m-TENG [115]. A surface charge density of 2380 μC /m^{-2} has been realized in ECE-TENG.

Aside from the contact efficiency, air breakdown is another factor that affects the performance of CE devices. Through continuous storage of charge from the e-TENG, the CEC can produce a vigorous electric field between the two electrodes of the m-TENG, causing the air to breakdown, so that the ionization charge deposited on the dielectric can subsequently diminish the ECE-TENG performance. Fortunately, by utilizing high dielectric strength dielectric oil to stuff the air gap, the air breakdown can be prevented during ECE-TENG operation. As displayed in figure 7(d), the performance of the proposed non-contact mode ECE-TENG with dielectric oil filling can reach 260.15 μC m^{-2}, which sets the output milestone for non-contact mode TENG [116]. Interestingly, the charge generated by air ionization in the m-TENG dielectric can be employed for increasing the surface charge density of the dielectric. By changing the polarity of the CEC, positive or negative charges can be deposited on the dielectric [68], as shown in figure 7(e). Once the up and down electrodes of the m-TENG are connected in an ordinary contact-separation TENG, the deposited charge can be outputted by electrostatic induction during contact separation.

3.3. SCE

In spite of the fact that ECP-TENG and ECE-TENG have achieved significant progress in boosting the TENG surface charge density, the introduction of pump generator and excitation generator has undoubtedly improved the complexity of the device structure. Taking inspiration from the concept of self-powered, SCE-TENG was proposed for increasing surface charge density by utilizing its output charge [114]. As well as having an ultra-high performance, SCE-TENG features a simplified device structure and a VMC (with a Zener diode) similar to ECE-TENG. Figure 8(a) illustrates the device diagram and the operating principle of SCE-TENG. The SCE-TENG structure is identical to the traditional TENG structure. As with ECP-TENG and ECE-TENG, SCE-TENG generates alternating current through charge transfer between a variable

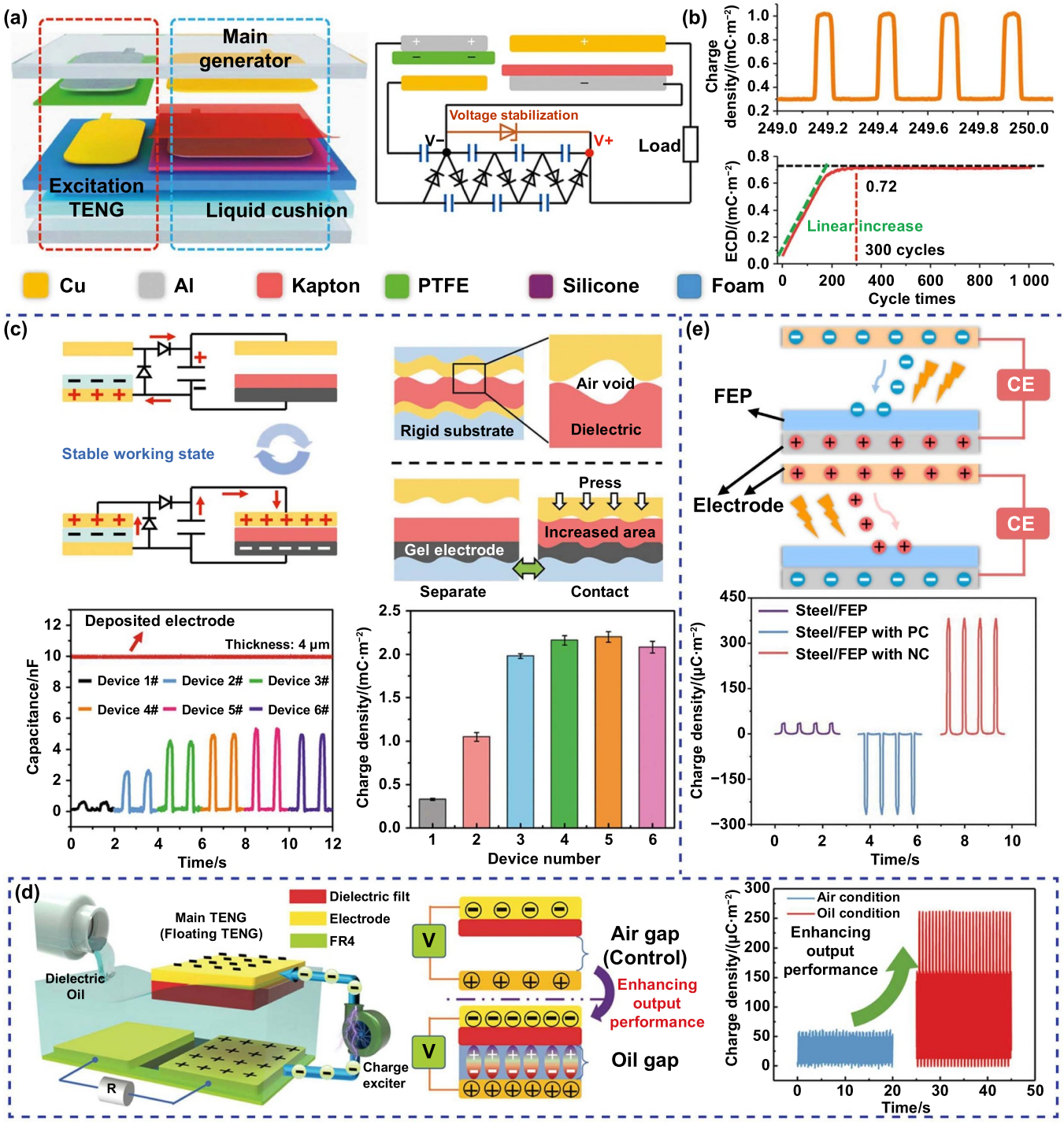

Figure 7. External charge excitation strategy for high-performance TENG. (a)–(b) Device sketch and output of the ECE-TENG. (a)–(b) Reproduced from [114]. CC BY 4.0. (c) The output of ECE-TENG is optimized by circuit design and contact efficiency. (c) Reproduced from [115]. CC BY 4.0. (d) Non-contact mode SCE-TENG output is optimized through the utilization of high dielectric strength dielectric oil. (d) [116] John Wiley & Sons. © 2022 Wiley-VCH GmbH. (e) Deposition of charges on the dielectric film by an external charge excitation TENG. (e) [68] John Wiley & Sons. © 2022 Wiley-VCH GmbH.

capacitor (m-TENG) and external fixed capacitors. The difference is that during the motion of SCE-TENG, the fixed capacitors automatically switch between the series-parallel state consequently, creating a charge self-improving effect. Specifically, in the primary state, the capacitance and charge of the m-TENG are regarded as $2C$ and $2Q$, respectively, whereas the corresponding parameters of the external capacitors are C and Q. As soon as the m-TENG is separated, its capacitance rapidly reduces to C_L. This will increase the voltage V of the m-TENG, causing a $2Q-Q'$ charge transfer to the fixed capacitors, resulting in a voltage balance state. Here Q' is the time-varying charge of the m-TENG and the fixed capacitors are

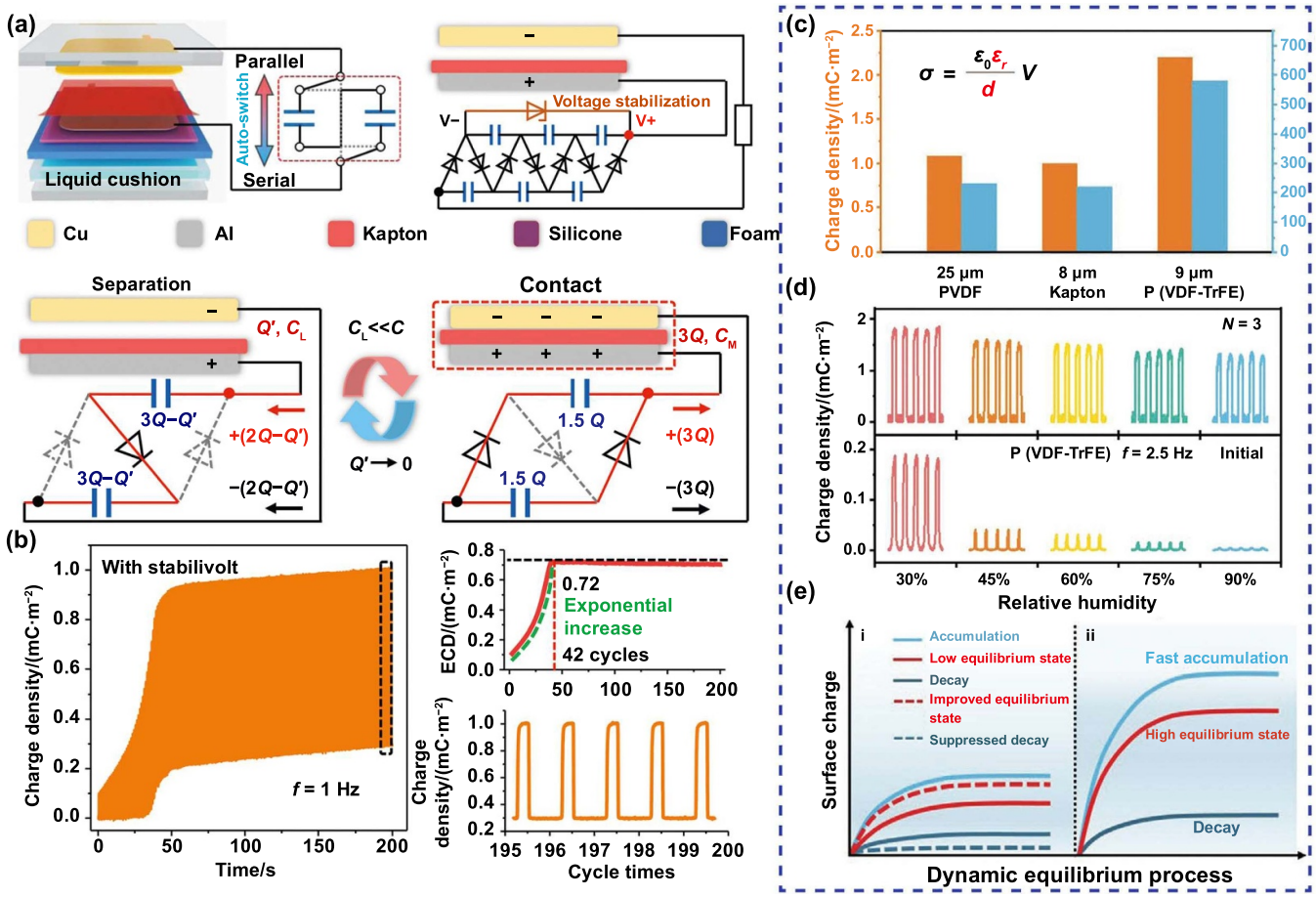

Figure 8. Self-charge excitation strategy for high-performance TENG. (a)–(b) Device sketch and performance of the SCE-TENG. (a)–(b) Reproduced with permission [114]. Copyright 2019, Springer Nature. (c) Charge density of the SCE-TENG based on various dielectrics. (d) Output performance of the SCE-TENG based on PVDF-TrFE at varying humidity. (e) Rapid charge accumulation of SCE-TENG. (c)–(e) Reproduced with permission [67]. Copyright 2021, Wiley-VCH GmbH. Reproduced from [114]. CC BY 4.0. [67] John Wiley & Sons. © 2021 Wiley-VCH GmbH.

in series during this process. When the separation distance is relatively large, C_L (the capacitance value of m-TENG in the separated status) is much smaller than C, so it can be assumed that Q' equals 0. The total charge of $2Q$ in the main TENG will be transported to the external capacitors, which will eventually total 3Q. As soon as the main TENG is in contact again, its capacitance increases to C_M (maximum capacitance value of main TENG). At this time, the external capacitors charge the main TENG and they are automatically switched into parallel. The theoretical calculation indicates that $3Q$ (1.5 times) of charge will be transported back to the m-TENG to accomplish charge self- improving. Figure 8(b) shows the output of SCE-TENG, where the ECD reaches a maximum of 0.72 mC m^{-2} after only 42 cycles, much less than the 300 cycles required to externally charge-stimulate the TENG (figure 7(b)).

Further improvement of the effective charge density of SCE-TENG was achieved through optimization of the properties of the dielectric film [67]. As presented in figure 8(c), 25 μm PVDF film (dielectric constant: 7.5), 8 μm Kapton film (dielectric constant: 3.7), and 9 μm PVDF-TrFE film (dielectric constant: 11.1) were utilized as the dielectric, respectively. As expected, the output of SCE-TENG can reach 2.20 mC m^{-2} using PVDF-TrFE with a smaller thickness and higher dielectric constant. A further investigation of the output of PVDF-TrFE-based SCE-TENG in a high RH environment can be seen in figure 8(d). An ordinary TENG based on PVDF-TrFE has weak output signals of approximately 0.005 mC m^{-2} at 90% relative humidity, whereas SCE-TENG based on PVDF-TrFE could achieve a charge density up to 1.3 mC m^{-2}, nearly 260 times greater than the former. The excellent performance of SCE-TENG under high humidity can be attributed to the fast accumulation of charges and the reduction of charge decay with the assistance of a VMC, as shown in figure 8(e).

SCE-TENG still experiences the air breakdown and charge deposition phenomenon due to the VMC generating vigorous voltage during operation [117], as shown in figure 9(a). The process of deposition of charges consists of four stages, with stage (i) representing TENG's original state without charge excitation. Since the electrode and dielectric contact is insufficient, there is only a small amount of triboelectric charge produced by the contact electrification. When the contact separation continues in stage (ii), charge migration and accumulation continuously occur between the VMC and m-TENG, resulting in enhancements in the excitation voltage across the VMC.

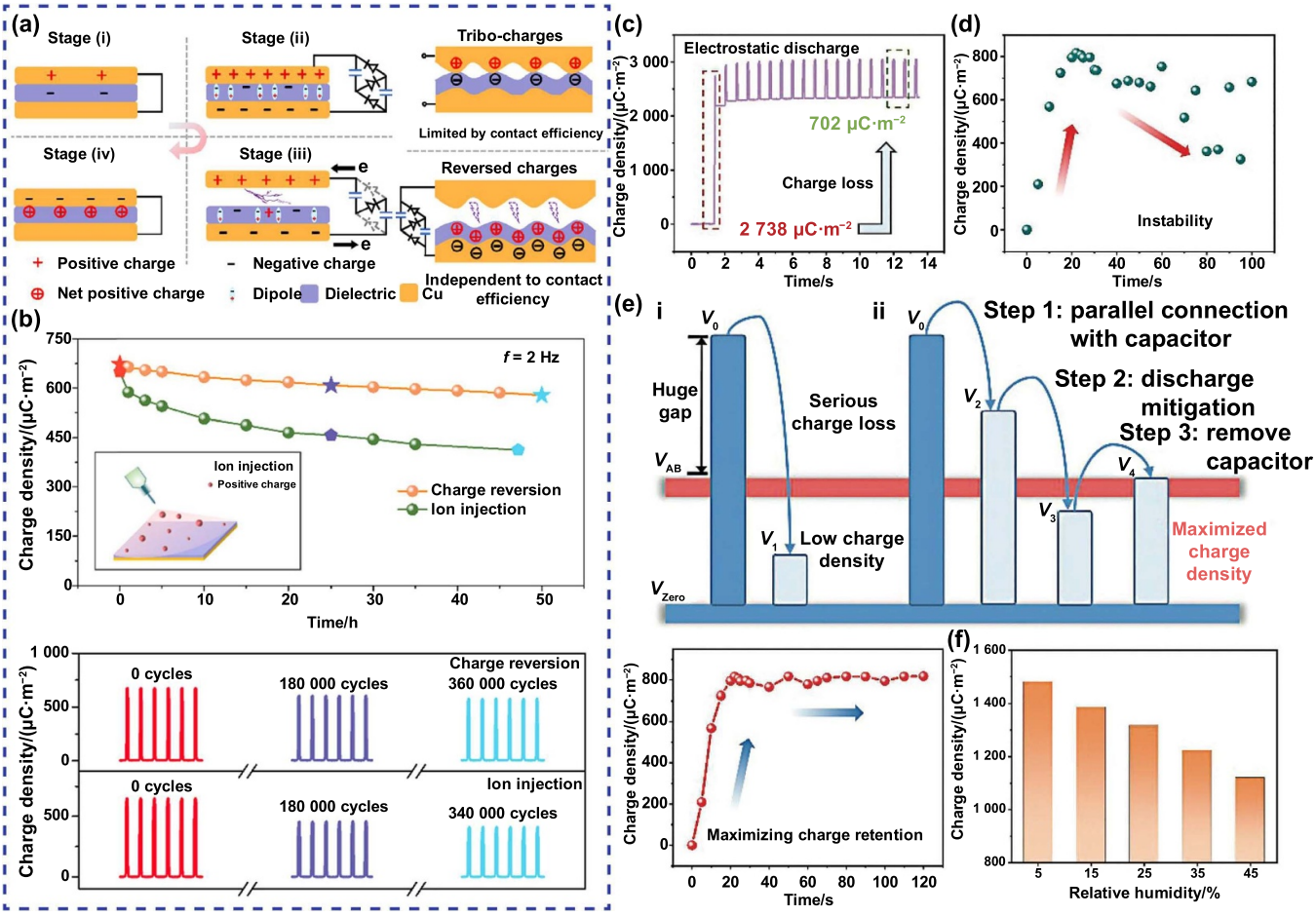

Figure 9. Increasing the surface charge density of dielectric materials by charge deposition. (a) Charge reversion process of SCE-TENG. (b) Stability of deposited charges. (a)–(b) Reproduced from [117] with permission from the Royal Society of Chemistry. (c)–(e) A charge migration strategy is proposed to stabilize deposited charges. (f) The influence of humidity on deposited charges. (c)–(f) [118] John Wiley & Sons. © 2023 Wiley-VCH GmbH.

Eventually, the breakdown of air occurs when the voltage between the counter electrode and the dielectric reaches a threshold value. A continuous decrease in exchange charge between TENG and VMC occurs at this point as a result of partial air ionization (stage iii). When the air breakdown phenomenon and ionization continue to occur, the charges generated by air ionization accumulate on the dielectric, resulting in a reversal of the polarity of the charges on the polymer. Subsequently, when disconnected from the VMC, the surface charge of the dielectric becomes positive as compared to its initial state, as shown in stage (iv). Unlike conventional contact electrification where the amount of charge is limited by the contact status, the charge deposition process in SCE-TENG is unrestricted by the contact status, thus allowing the surface charge density of the dielectric to improve greatly. Additionally, the long-term durability of the TENG with deposited charge as the output source was investigated (figure 9(b)) and compared with the output of the ion injection method. After 180 000 operation cycles, the performance of the TENG (charge source from the deposited charge during the SCE process) could keep at 89.7% (604 μC m^{-2}), and after 360 000 cycles, the output still maintained 85.1% (573 μC m^{-2}). By comparison, the ion injection method could hold 63.5% (410 μC m^{-2}) after 340 000 cycles, indicating that the TENG with SCE-deposited charge has greater stability than the ion injection method.

By directly depositing charges on the dielectric through the SCE process, the surface charge density of TENG devices is remarkably enhanced. Nevertheless, since the dielectric surface is highly charged after charge deposition, most of the deposited charge is lost during startup [118], as depicted in figure 9(c). This is because the primal voltage (V_0) produced by the deposited charge is greater than the air breakdown threshold (V_{AB}), resulting in an electrostatic discharge that ultimately retains an output of 702 μC m^{-2}. Figure 9(d) illustrates the output charge density after different charge deposition times, and it is apparent that the more charges deposited, the greater the electrostatic discharge, which causes a lower output charge density. To address this shortcoming, a discharge mitigation strategy is attempted, as illustrated in figure 9(e). After electrostatic discharge, V_0 decreases significantly, as portrayed in figures 9(e)–(i), due to the significant difference between V_0 and V_{AB}. A parallel connection between an external capacitor and the TENG with deposited

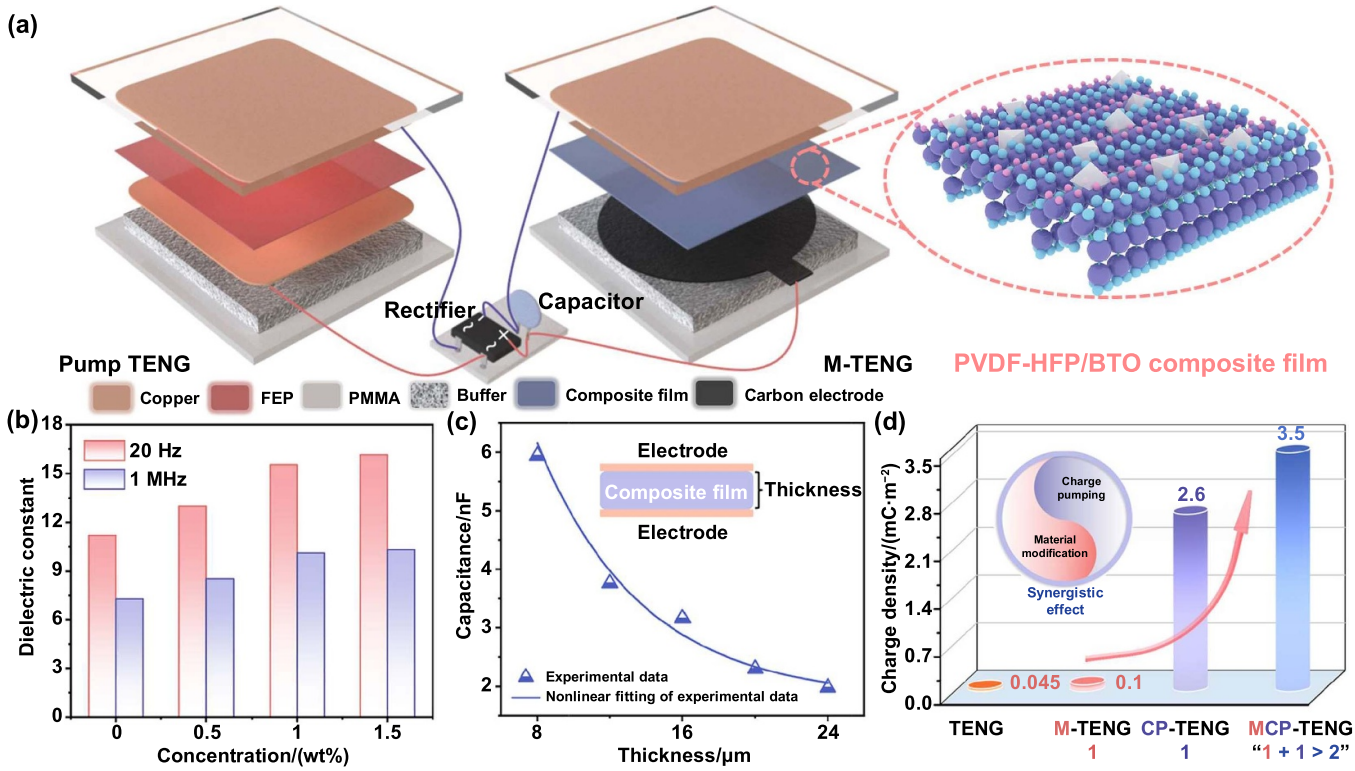

Figure 10. Increasing the output of ECP-TENG through material modification. (a) Device configuration of MCP-TENG based on PVDF-HFP/BTO. (b)–(c) The dielectric constant and capacitance of PVDF-HFP/BTO. (d) Performance comparison of four types of TENG. (a)–(d) Reprinted from [119], © 2024 Elsevier B.V. All rights reserved.

charge allows the degree of discharge during initial contact to be reduced, as portrayed in figure 9(e-ii). As can be seen, using the discharge mitigation strategy, a remarkable improvement in the output stability of the deposited charge is achievable. With further control of the RH, as presented in figure 9(f), the charge density of the Polyimide (PI) film can be as high as 1.48 mC m^{-2} (at 5% RH).

4. Strategy conjunction

As discussed above, material optimization and circuit design could boost the surface charge density from different perspectives. With material modification, a variety of novel materials can be introduced into the material system for TENGs, and the properties of triboelectric dielectric (e.g. surface state, polarization, dielectric constant, leakage current, etc) can be effortlessly tuned. The advantage of the CP and charge excitation strategies could greatly raise the upper output limit. An optimized strategy from these enhancement methods could deliver a higher surface charge density. In addition, the physical properties of the dielectric materials under strong excitation electric fields can also be actively explored.

It has recently been reported to utilize material modification and CP synergy to construct ultra-high charge density TENG (MCP-TENG) [119], as demonstrated in figure 10(a). Unlike the commercially available dielectric (Polypropylene and PI) previously reported to be employed by ECP-TENG, poly(vinylidene fluoride-co-hexafluoropropylene) (PVDF-HFP) film with the tunability of the electrical properties was employed as the dielectric polymer for the newly MCP-TENG. By doping BTO, as presented in figure 10(b), PVDF-HFP can be enhanced in the dielectric constant, thereby increasing the contact capacitance. Note that as the doping content increases, the nanoparticles could aggregate on the dielectric, thereby affecting the contact efficiency. As a result, 1 wt% BTO was found to be the optimal content of doping. Furthermore, the thickness of the PVDF-HFP/BTO was reduced to enhance the actual contact capacitance, as illustrated in figure 10(c). As a result, the MCP-TENG fabricated using the optimal PVDF-HFP/BTO composite can output a charge density of 3500 μC m^{-2}, higher than the sum of the charge density obtained by M-TENG (PVDF-HFP as dielectric) and ECP-TENG (PVDF-HFP as dielectric), implying that the demonstrated synergies for ultra-high performance TENGs are feasible and achievable, as displayed in figure 10(d).

A combination of the e-TENG and the CEC can continuously generate an intense voltage between the two electrodes of the m-TENG during the CE process. This phenomenon could cause the disordered dipole moment in the PVDF film between the two electrodes of the m-TENG to polarize by gradually deflecting along the direction of the electric field, increasing the permittivity of the thin film [65], as presented in figure 11(a). In this periodic self-polarization manner, the capacitance of the m-TENG could amplify as the ECE-TENG continues to operate, as could the output charge

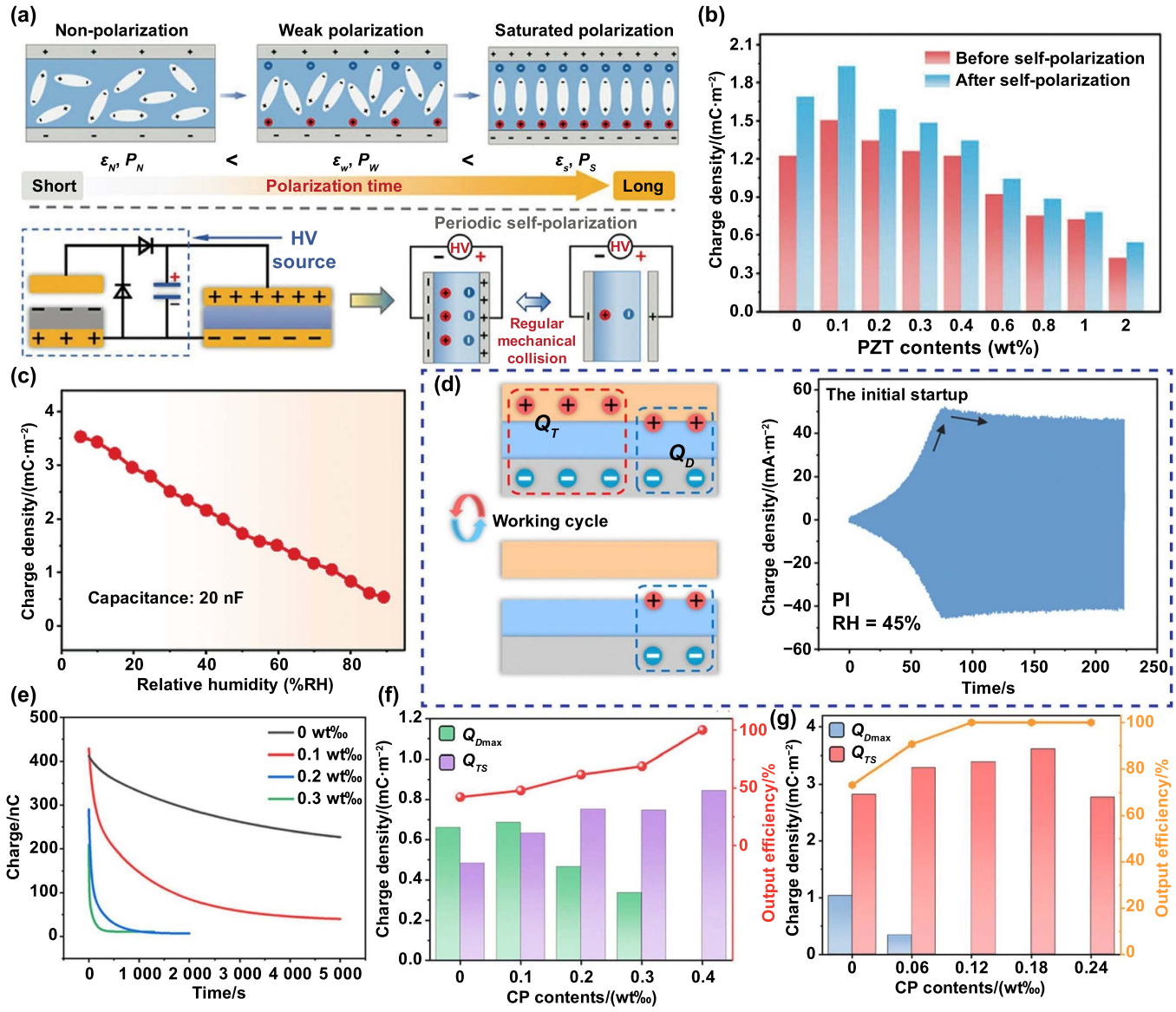

Figure 11. Improving the performance of ECE-TENG through material optimization. (a) Self-polarization phenomenon of dielectric in ECE-TENG. (b) Charge density of ECE-TENG based on PVDF/PZT. (c) The effect of RH on the charge density of ECE-TENG. (a)–(c) [65] John Wiley & Sons. © 2022 Wiley-VCH GmbH. (d) The effect of air breakdown phenomenon on the output of ECE-TENG. (e) The charge attenuation of PI/CP composite thin films. (f) Output charge and efficiency of ECE-TENG based on PI/CP composite. (g) Output charge and efficiency of ECE-TENG based on PVDF/CP composite. (d)–(g) Reproduced from [120] with permission from the Royal Society of Chemistry.

density. By adding lead zirconate titanate (PZT) powder to PVDF, the output of ECE-TENG is further boosted before and after self-polarization. The maximum charge density of the thin film with a PZT concentration of 0.1 wt% was 1.93 mC m^{-2}, as presented in figure 11(b). When RH is well controlled, as demonstrated in figure 11(c), ECE-TENG based on PVDF/PZT composite can achieve charge density above 3500 μC m^{-2}, which is considerably higher than the maximum output previously achieved by ECE-TENG using unmodified dielectric thin film (figure 7(c)). As shown in figure 11(d), the output of the ECE-TENG is impeded by the air breakdown phenomenon. One solution is to introduce some conductive materials, such as carbon powder (CP), to the dielectric to render the charge trapping of the dielectric film [120]. With an increase in CP content, as depicted in figure 11(e), the charge decay of the CP/PI composite rises significantly and the trap energy level decreases. Figure 11(f) illustrates the effect of CP filling concentrations of 0.4 wt% in reducing the deposited charge on CP/PI film caused by air breakdown, resulting in 100% output efficiency for the composite film-based ECE-TENG. When PVDF is employed instead of PI, the ECE-TENG output charge density based on PVDF/CP composite film can be 4.13 mC m^{-2}, further demonstrating the success of material modification and circuit design synergy in improving TENG surface charge density, as illustrated in figure 11(g).

Besides improving the performance of ECE-TENG and ECP-TENG, material modification can also boost SCE-TENG

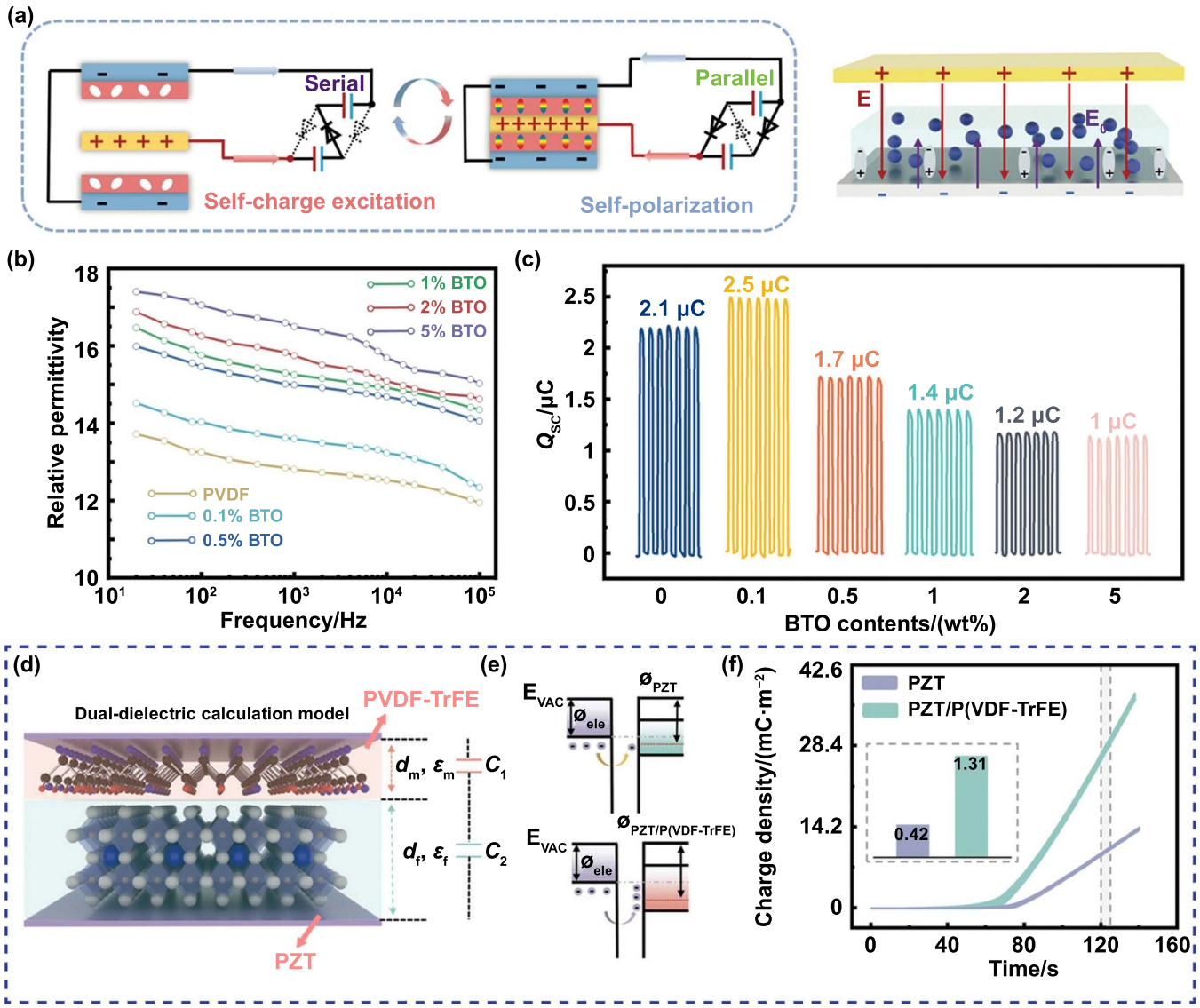

Figure 12. Enhancing the charge density of SCE-TENG through material modulation. (a) Self-polarization of dielectric film in SCE-TENG. (b) The dielectric constant of PVDF/BTO. (c) Output of SCE-TENG (PVDF/BTO as a dielectric). (a)–(c) [64] John Wiley & Sons. © 2022 Wiley-VCH GmbH. (d) Equivalent capacitance of PVDF-TrFE/PZT composite dielectric. (e) The band structure of PVDF-TrFE/PZT composite. (f) Charge density of SCE-TENG based on PVDF-TrFE/PZT composite. (d)–(f) [66] John Wiley & Sons. © 2023 Wiley-VCH GmbH.

performance. A strong electric field is produced at both ends of VMC during the operation of the CE process, so the self-polarization phenomena of polar dielectrics are also observed in SCE-TENG (figure 12(a)) [64]. BTO nanoparticles with high dielectric constant were then embedded to the PVDF film to increase its polarization capability and dielectric constant, as shown in figure 12(b). Consequently, when the concentration of BTO nanoparticles is 0.1 wt%, the output charge of SCE-TENG can reach 2.5 μC. There has been a remarkable improvement in the charge density in comparison to the previous use of unmodified materials in SCE-TENG (figure 8(b)). In addition to polymer dielectric materials, some inorganic bulk materials with high dielectric constants, such as PZT, have also been investigated for high output SCE-TENG [66], as depicted in figure 12(d). During contact, only a small amount of charge is transferred to the bulk material because the difference in the work functions between electrode and PZT is not significant (figure 12(f)). For this reason, coating of a thin layer of PVDF-TrFE onto the PZT could strengthen its contact electrification capability. Therefore, the SCE-TENG constructed with PZT/PVDF-TrFE yields an output of 1.31 mC m^{-2}, which is approximately 68% greater than that of the SCE-TENG constructed with pure PZT. Additionally, The charge density and power density of ECP-TENG, ECE-TENG, and SCE-TENG with different dielectrics are summarized in table 2. And figure 13 also compares the maximum surface charge density achieved by currently employing material modification, circuit design,

Table 2. Comparison of ECP-TENG, ECE-TENG, and SCE-TENG fabricated from different dielectrics.

TENG types	Dielectric material	Counter layer	Charge density (mC m^{-2})	Power density (W m^{-2})	References
ECP-TENG	PVDF/EP	PVDF/EP	0.49	—	[60]
	PP	Cu	1.02	20	[69]
	PP	Zn-Al	1.85	13.3	[112]
	PET	Permalloy	2.85	42	[61]
	PVDF-HFP/BTO	Cu	3.5	61.2	[119]
ECE-TENG	PI	Cu	0.81	38.2	[114]
	PVDF/PI	Cu	2.2	61.3	[121]
	PEI	Cu	2.38	115.6	[115]
	PVDF/PZT	Stainless steel	3.5	142.5	[65]
	PVDF/CP	Stainless steel	4.0	58.2	[120]
	PI	Stainless steel	0.88	9.04	[68]
	PI	Cu	0.26	6.2	[116]
	PVDF-TrFE	Stainless steel	2.88	25.84	[122]
SCE-TENG	PVDF/BTO	Stainless steel	1.67	14.22	[64]
	PVDF-TrFE/PZT	Stainless steel	1.31	10.96	[66]
	PVDF-TrFE	Cu	2.2	40.0	[67]
	PTFE	Cu	0.212	6.5	[116]
	PI	Stainless steel	1.48	86	[118]
	PTFE	Cu	0.78	—	[117]

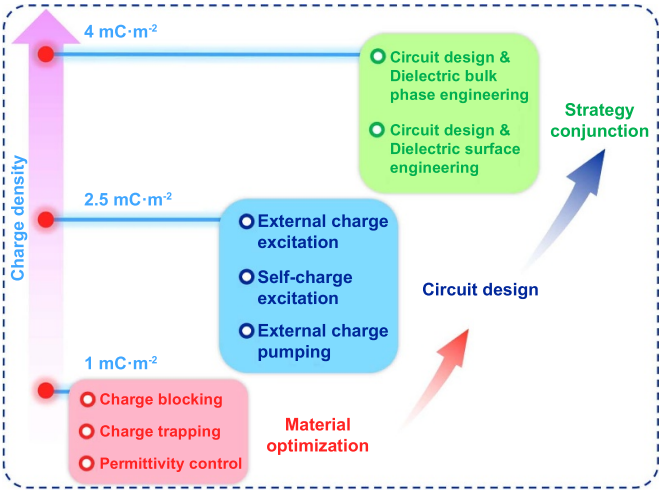

Figure 13. Comparison of maximum surface charge density achieved by different strategies in vertical contact-separation TENG.

or strategy conjunction in the vertical contact-separation TENG.

5. Summary and perspective

An in-depth and systematic retrospection of recent developments in the manufacture of high-performance TENG is summarized in this review. It can be seen that triboelectric dielectric materials that have strong charge storage capabilities are ideal candidates for the manufacture of high-output TENG. With reasonable external circuit design and assistance, the surface charge density will surpass the air breakdown limit and reach over 1 mC m^{-2}. These efforts are progressing energy harvesting techniques, as well as exploring and applying traditional dielectric polymer materials and novel materials in new energy fields. It is conceivable that with the continuous advancement of TENG performance and the expansion of application scenarios, TENGs could have a revolutionary impact on our production and our lives [123–126]. However, toward this destination, several challenges require additional efforts in order for the sustainable development of high charge density TENGs.

Charge storage mechanism. As of today, many physical models interpret the charge transfer process between two materials. However, interpretations of the transport, storage, and attenuation of triboelectric charges on the dielectrics are still under debate. It has been reported that the subsequent behavior of these triboelectric charges on the dielectrics has a significant impact on charge transfer on the surfaces of the dielectrics. In-depth research on triboelectric charge behavior as well as the establishment of physical models describing charge migration on dielectric surfaces would enrich the basic theory of TENG.

Eco-friendly triboelectric materials. Some polymer materials used in TENGs are difficult to degrade naturally, and this raises an environmental concern. As such, it is imperative that triboelectric materials be developed that are of high charge density and stability, as well as both eco-friendly and biodegradable. Most of the materials that are being employed as dielectric layers for TENGs at present are organic materials. Inorganic materials with high dielectric constants, as well as novel inorganic materials, should also be explored for this purpose.

Durability. It is very important to take into account the reliability and durability of a TENG. Wear and tear of the dielectrics and electrode materials in a TENG inevitably occurs during the triboelectrification process, leading to a

decline in performance. Therefore, the development of triboelectric dielectrics with high wear and tear resistance is in high demand. In addition, advanced TENG structural designs to avoid hard wear and tear can be another way out.

Circuit enhancement technology for TENGs. With the introduction of CP and charge excitation techniques, the output of TENGs has been significantly boosted. However, optimizations of a variety of operating modes and structural designs are necessary to achieve high performance for most TENG modes.

Performance test criteria. Even though TENG has been developed for many years, the standards for characterization of TENGs and assessment of their performance are still lacking. To quantify the performance of TENG, environmental variables (temperature, humidity, pressure, and gas types), test variables (force, frequency, velocity, acceleration, charge accumulation time, and contact efficiency), and device preparation variables (flexible electrodes, rigid electrodes, softness and hardness of the buffer layer, and so on) should be further classified and standardized.

Power management. Efficiently transmitting, managing, and storing the high-density energy from TENGs is necessary to expand their practical applications. Enhancement of the efficiency of the power management module in electric power transmission and management is a key for practical application. To store harvested electric energy in chemical electricity storage devices (supercapacitors or batteries), it is essential to convert the transient voltage pulses generated from a TENG into a DC current for charging the devices. In addition, smart power management could play a role in the integration of individual TENGs into a large array of TENGs for a large scale of mechanical energy harvesting.

Acknowledgments

This work was supported by the National Key R & D Project from the Ministry of Science and Technology, China (2021YFA1201603), NSFC (52073032 and 52192611) and the Fundamental Research Funds for the Central Universities.

ORCID iD

Junyi Zhai https://orcid.org/0000-0001-8900-4638

References

[1] Chu S, Cui Y and Liu N 2016 The path towards sustainable energy *Nat. Mater.* **16** 16–22
[2] Shen L, Jacob D J, Gautam R, Omara M, Scarpelli T R, Lorente A, Zavala-Araiza D, Lu X, Chen Z C and Lin J T 2023 National quantifications of methane emissions from fuel exploitation using high resolution inversions of satellite observations *Nat. Commun.* **14** 4948
[3] Achakulwisut P, Erickson P, Guivarch C, Schaeffer R, Brutschin E and Pye S 2023 Global fossil fuel reduction pathways under different climate mitigation strategies and ambitions *Nat. Commun.* **14** 5425
[4] Yang H Z, Deshmukh R and Suh S 2023 Global transcontinental power pools for low-carbon electricity *Nat. Commun.* **14** 8350
[5] Murunga M, Macleod C and Pecl G 2024 Assumptions and contradictions shape public engagement on climate change *Nat. Clim. Change* **14** 126–33
[6] Davidson D J 2019 Exnovating for a renewable energy transition *Nat. Energy* **4** 254–6
[7] Meckling J, Galeazzi C, Shears E, Xu T and Anadon L D 2022 Energy innovation funding and institutions in major economies *Nat. Energy* **7** 876–85
[8] Guan Y R *et al* 2023 Burden of the global energy price crisis on households *Nat. Energy* **8** 304–16
[9] Yao Z P, Lum Y, Johnston A, Mejia-Mendoza L M, Zhou X, Wen Y G, Aspuru-Guzik A, Sargent E H and Seh Z W 2023 Machine learning for a sustainable energy future *Nat. Rev. Mater.* **8** 202–15
[10] Qian H Q, Xu S D, Cao J, Ren F Z, Wei W D, Meng J and Wu L B 2021 Air pollution reduction and climate co-benefits in China's industries *Nat. Sustain.* **4** 417–25
[11] Fan F R, Tian Z Q and Wang Z L 2012 Flexible triboelectric generator *Nano Energy* **1** 328–34
[12] Guo H Y, Yeh M H, Lai Y C, Zi Y L, Wu C S, Wen Z, Hu C G and Wang Z L 2016 All-in-one shape-adaptive self-charging power package for wearable electronics *ACS Nano* **10** 10580–8
[13] Zhao K, Wang Y H, Han L, Wang Y F, Luo X D, Zhang Z Q and Yang Y 2019 Nanogenerator-based self-charging energy storage devices *Nano-Micro Lett.* **11** 19
[14] Liu R Y, Wang Z L, Fukuda K and Someya T 2022 Flexible self-charging power sources *Nat. Rev. Mater.* **7** 870–86
[15] Jiang C M, Li X J, Lian S W M, Ying Y B, Ho J S and Ping J F 2021 Wireless technologies for energy harvesting and transmission for ambient self-powered systems *ACS Nano* **15** 9328–54
[16] Xu C, Song Y, Han M D and Zhang H X 2021 Portable and wearable self-powered systems based on emerging energy harvesting technology *Microsyst. Nanoeng.* **7** 25
[17] Fu X P, Xu S H, Gao Y Y, Zhang X H, Liu G X, Zhou H, Lv Y, Zhang C and Wang Z L 2021 Breeze-wind-energy-powered autonomous wireless anemometer based on rolling contact-electrification *ACS Energy Lett.* **6** 2343–50
[18] Zhang X, Li Z K, Du W W, Zhao Y L, Wang W, Pang L L, Chen L, Yu A F and Zhai J Y 2022 Self-powered triboelectric-mechanoluminescent electronic skin for detecting and differentiating multiple mechanical stimuli *Nano Energy* **96** 107115
[19] Wang W, Yu A F, Wang Y L, Jia M M, Guo P W, Ren L L, Guo D, Pu X, Wang Z L and Zhai J Y 2022 Elastic kernmantle e-braids for high-impact sports monitoring *Adv. Sci.* **9** 2202489
[20] Xu L *et al* 2018 Giant voltage enhancement *via* triboelectric charge supplement channel for self-powered electroadhesion *ACS Nano* **12** 10262–71
[21] Meng X C, Xiao X, Jeon S, Kim D, Park B J, Kim Y J, Rubab N, Kim S M and Kim S W 2023 An ultrasound-driven bioadhesive triboelectric nanogenerator for instant wound sealing and electrically accelerated healing in emergencies *Adv. Mater.* **35** 2209054
[22] Imani I M, Kim B, Xiao X, Rubab N, Park B J, Kim Y J, Zhao P, Kang M and Kim S W 2023 Ultrasound-driven on-demand transient triboelectric nanogenerator for subcutaneous antibacterial activity *Adv. Sci.* **10** 2204801
[23] Ouyang H *et al* 2019 Symbiotic cardiac pacemaker *Nat. Commun.* **10** 1821
[24] Zheng Q *et al* 2016 *In vivo* self-powered wireless cardiac monitoring via implantable triboelectric nanogenerator *ACS Nano* **10** 6510–8

[25] Yang D, Ni Y F, Kong X X, Li S Y, Chen X Y, Zhang L Q and Wang Z L 2021 Self-healing and elastic triboelectric nanogenerators for muscle motion monitoring and photothermal treatment *ACS Nano* **15** 14653–61
[26] Yang J, An J, Sun Y S, Zhang J J, Zu L L, Li H, Jiang T, Chen B D and Wang Z L 2022 Transparent self-powered triboelectric sensor based on PVA/PA hydrogel for promoting human-machine interaction in nursing and patient safety *Nano Energy* **97** 107199
[27] Wei C H, Cheng R W, Ning C, Wei X Y, Peng X, Lv T M, Sheng F F, Dong K and Wang Z L 2023 A self-powered body motion sensing network integrated with multiple triboelectric fabrics for biometric gait recognition and auxiliary rehabilitation training *Adv. Funct. Mater.* **33** 2303562
[28] Shi Y X, Yang P, Lei R, Liu Z Q, Dong X Y, Tao X L, Chu X C, Wang Z L and Chen X Y 2023 Eye tracking and eye expression decoding based on transparent, flexible and ultra-persistent electrostatic interface *Nat. Commun.* **14** 3315
[29] Liu D, Zhang D L, Sun Z R, Zhou S Y, Li W, Li C Y, Li W S, Tang W and Wang Z L 2022 Active-matrix sensing array assisted with machine-learning approach for lumbar degenerative disease diagnosis and postoperative assessment *Adv. Funct. Mater.* **32** 2113008
[30] Lu Y J, Tian H, Cheng J, Zhu F, Liu B, Wei S S, Ji L H and Wang Z L 2022 Decoding lip language using triboelectric sensors with deep learning *Nat. Commun.* **13** 1401
[31] Wei X L, Wang B C, Cao X L, Zhou H L, Wu Z Y and Wang Z L 2023 Dual-sensory fusion self-powered triboelectric taste-sensing system towards effective and low-cost liquid identification *Nat. Food* **4** 721–32
[32] Lan L Y, Xiong J Q, Gao D C, Li Y, Chen J, Lv J, Ping J P, Ying Y B and Lee P S 2021 Breathable nanogenerators for an on-plant self-powered sustainable agriculture system *ACS Nano* **15** 5307–15
[33] Li X J, Luo J J, Han K, Shi X, Ren Z W, Xi Y, Ying Y B, Ping J F and Wang Z L 2022 Stimulation of ambient energy generated electric field on crop plant growth *Nat. Food* **3** 133–42
[34] Yang H X, Miao X, Li Z K, Cui W Q, Zhao Y L, Cheng M F, Yu A F and Zhai J Y 2024 Earthworm-inspired triboelectric nanogenerator with O-shaped multilayer structure for marine ranching *Energy Technol.* **12** 2300819
[35] Cao X L, Wei X L, Huo X Q, Wang B C, Hu Y R, Wang Z L and Wu Z Y 2023 Self-powered retractable reel sensor for crack monitoring and warning in civil infrastructures *Chem. Eng. J.* **478** 147238
[36] Xia K Q, Fu J M and Xu Z W 2020 Multiple-frequency high-output triboelectric nanogenerator based on a water balloon for all-weather water wave energy harvesting *Adv. Energy Mater.* **10** 2000426
[37] Zhao T C, Xu M Y, Xiao X, Ma Y, Li Z and Wang Z L 2021 Recent progress in blue energy harvesting for powering distributed sensors in ocean *Nano Energy* **88** 106199
[38] Liang X, Jiang T, Liu G X, Feng Y W, Zhang C and Wang Z L 2020 Spherical triboelectric nanogenerator integrated with power management module for harvesting multidirectional water wave energy *Energy Environ. Sci.* **13** 277–85
[39] Zhang C G, Liu L, Zhou L L, Yin X, Wei X L, Hu Y X, Liu Y B, Chen S Y, Wang J and Wang Z L 2020 Self-powered sensor for quantifying ocean surface water waves based on triboelectric nanogenerator *ACS Nano* **14** 7092–100
[40] Xiao T X, Liang X, Jiang T, Xu L, Shao J J, Nie J H, Bai Y, Zhong W and Wang Z L 2018 Spherical triboelectric nanogenerators based on spring-assisted multilayered structure for efficient water wave energy harvesting *Adv. Funct. Mater.* **28** 1802634
[41] Wang Z L 2023 Nanogenerators and piezotronics: from scientific discoveries to technology breakthroughs *MRS Bull.* **48** 1014–25
[42] Wang S H, Zi Y L, Zhou Y S, Li S M, Fan F R, Lin L and Wang Z L 2016 Molecular surface functionalization to enhance the power output of triboelectric nanogenerators *J. Mater. Chem.* A **4** 3728–34
[43] Song G *et al* 2015 Molecularly engineered surface triboelectric nanogenerator by self-assembled monolayers (METS) *Chem. Mater.* **27** 4749–55
[44] Lin S Q, Zheng M L, Luo J J and Wang Z L 2020 Effects of surface functional groups on electron transfer at liquid-solid interfacial contact electrification *ACS Nano* **14** 10733–41
[45] Li S Y, Nie J H, Shi Y X, Tao X L, Wang F, Tian J W, Lin S Q, Chen X Y and Wang Z L 2020 Contributions of different functional groups to contact electrification of polymers *Adv. Mater.* **32** 2001307
[46] Liu Y H, Mo J L, Fu Q, Lu Y X, Zhang N, Wang S F and Nie S X 2020 Enhancement of triboelectric charge density by chemical functionalization *Adv. Funct. Mater.* **30** 2004714
[47] Lin Z H, Zhu G, Zhou Y S, Yang Y, Bai P, Chen J and Wang Z L 2013 A self-powered triboelectric nanosensor for mercury ion detection *Angew. Chem., Int. Ed.* **52** 5065–9
[48] Lin L, Wang S H, Xie Y N, Jing Q S, Niu S M, Hu Y F and Wang Z L 2013 Segmentally structured disk triboelectric nanogenerator for harvesting rotational mechanical energy *Nano Lett.* **13** 2916–23
[49] Yang W Q, Chen J, Zhu G, Wen X N, Bai P, Su Y J, Lin Y and Wang Z L 2013 Harvesting vibration energy by a triple-cantilever based triboelectric nanogenerator *Nano Res.* **6** 880–6
[50] Li Z L, Chen J, Yang J, Su Y J, Fan X, Wu Y, Yu C W and Wang Z L 2015 β-cyclodextrin enhanced triboelectrification for self-powered phenol detection and electrochemical degradation *Energy Environ. Sci.* **8** 887–96
[51] Lin Z H, Cheng G, Li X H, Yang P K, Wen X N and Wang Z L 2015 A multi-layered interdigitative-electrodes-based triboelectric nanogenerator for harvesting hydropower *Nano Energy* **15** 256–65
[52] Wang S H, Lin L and Wang Z L 2012 Nanoscale triboelectric-effect-enabled energy conversion for sustainably powering portable electronics *Nano Lett.* **12** 6339–46
[53] Zhu G, Lin Z H, Jing Q S, Bai P, Pan C F, Yang Y, Zhou Y S and Wang Z L 2013 Toward large-scale energy harvesting by a nanoparticle-enhanced triboelectric nanogenerator *Nano Lett.* **13** 847–53
[54] Wang J, Wu C S, Dai Y J, Zhao Z H, Wang A, Zhang T J and Wang Z L 2017 Achieving ultrahigh triboelectric charge density for efficient energy harvesting *Nat. Commun.* **8** 88
[55] Cheng B L, Xu Q, Ding Y Q, Bai S, Jia X F, Yu Y D C, Wen J and Qin Y 2021 High performance temperature difference triboelectric nanogenerator *Nat. Commun.* **12** 4782
[56] Liu D *et al* 2022 Standardized measurement of dielectric materials' intrinsic triboelectric charge density through the suppression of air breakdown *Nat. Commun.* **13** 6019
[57] Liu Z Q, Huang Y Z, Shi Y X, Tao X L, He H Z, Chen F D, Huang Z X, Wang Z L, Chen X Y and Qu J P 2022 Fabrication of triboelectric polymer films via repeated rheological forging for ultrahigh surface charge density *Nat. Commun.* **13** 4083

[58] Liu Z Q, Huang Y Z, Shi Y X, Tao X L, Yang P, Dong X Y, Hu J, Huang Z X, Chen X Y and Qu J P 2023 Creating ultrahigh and long-persistent triboelectric charge density on weak polar polymer via quenching polarization *Adv. Funct. Mater.* **33** 2302164

[59] Li S Y, Fan Y, Chen H Q, Nie J H, Liang Y X, Tao X L, Zhang J, Chen X Y, Fu E G and Wang Z L 2020 Manipulating the triboelectric surface charge density of polymers by low-energy helium ion irradiation/implantation *Energy Environ. Sci.* **13** 896–907

[60] Cheng L, Xu Q, Zheng Y B, Jia X F and Qin Y 2018 A self-improving triboelectric nanogenerator with improved charge density and increased charge accumulation speed *Nat. Commun.* **9** 3773

[61] Qi Y C, Liu G X, Bu T Z, Zeng J H, Zhang Z and Zhang C 2022 Ferromagnetic-based charge-accumulation triboelectric nanogenerator with ultrahigh surface charge density *Small* **18** 2201754

[62] Meng J, Pan C X, Li L W, Guo Z H, Xu F, Jia L Y, Wang Z L and Pu X 2022 Durable flexible direct current generation through the tribovoltaic effect in contact-separation mode *Energy Environ. Sci.* **15** 5159–67

[63] Liu D, Gao Y K, Zhou L L, Wang J and Wang Z L 2023 Recent advances in high-performance triboelectric nanogenerators *Nano Res.* **16** 11698–717

[64] Wang J, Wu H Y, Wang Z, He W C, Shan C C, Fu S K, Du Y, Liu H and Hu C G 2022 An ultrafast self-polarization effect in barium titanate filled poly(vinylidene fluoride) composite film enabled by self-charge excitation triboelectric nanogenerator *Adv. Funct. Mater.* **32** 2204322

[65] Wu H Y, He W C, Shan C C, Wang Z, Fu S K, Tang Q, Guo H Y, Du Y, Liu W L and Hu C G 2022 Achieving remarkable charge density via self-polarization of polar high-k material in a charge-excitation triboelectric nanogenerator *Adv. Mater.* **34** 2109918

[66] Wang J, Li G, Xu S Y, Wu H Y, Fu S K, Shan C C, He W C, Zhao Q H, Li K X and Hu C G 2023 Remarkably enhanced charge density of inorganic material via regulating contact barrier difference and charge trapping for triboelectric nanogenerator *Adv. Funct. Mater.* **33** 2304221

[67] Li Y H, Zhao Z H, Liu L, Zhou L L, Liu D, Li S X, Chen S Y, Dai Y J, Wang J and Wang Z L 2021 Improved output performance of triboelectric nanogenerator by fast accumulation process of surface charges *Adv. Energy Mater.* **11** 2100050

[68] Wu H Y, Fu S K, He W C, Shan C C, Wang J, Du Y, Du S H, Li B X and Hu C G 2022 Improving and quantifying surface charge density via charge injection enabled by air breakdown *Adv. Funct. Mater.* **32** 2203884

[69] Xu L, Bu T Z, Yang X D, Zhang C and Wang Z L 2018 Ultrahigh charge density realized by charge pumping at ambient conditions for triboelectric nanogenerators *Nano Energy* **49** 625–33

[70] Seung W *et al* 2017 Boosting power-generating performance of triboelectric nanogenerators via artificial control of ferroelectric polarization and dielectric properties *Adv. Energy Mater.* **7** 1600988

[71] Choi Y S, Kim S W and Kar-Narayan S 2021 Materials-related strategies for highly efficient triboelectric energy generators *Adv. Energy Mater.* **11** 2003802

[72] Li Z K, Zhang L, Guo L H, Hu W Q, Yu A F and Zhai J Y 2023 Manipulating functional groups between polyvinylidene difluoride and nanoparticles for high-performance triboelectric nanogenerator *Nano Res.* **16** 11855–61

[73] Tao X L, Chen X Y and Wang Z L 2023 Design and synthesis of triboelectric polymers for high performance triboelectric nanogenerators *Energy Environ. Sci.* **16** 3654–78

[74] Niu S M, Liu Y, Wang S H, Lin L, Zhou Y S, Hu Y F and Wang Z L 2014 Theoretical investigation and structural optimization of single-electrode triboelectric nanogenerators *Adv. Funct. Mater.* **24** 3332–40

[75] Niu S M, Liu Y, Zhou Y S, Wang S H, Lin L and Wang Z L 2015 Optimization of triboelectric nanogenerator charging systems for efficient energy harvesting and storage *IEEE Trans. Electron. Devices* **62** 641–7

[76] Zi Y L, Niu S M, Wang J, Wen Z, Tang W and Wang Z L 2015 Standards and figure-of-merits for quantifying the performance of triboelectric nanogenerators *Nat. Commun.* **6** 8376

[77] Niu S M, Liu Y, Wang S H, Lin L, Zhou Y S, Hu Y F and Wang Z L 2013 Theory of sliding-mode triboelectric nanogenerators *Adv. Mater.* **25** 6184–93

[78] Niu S M, Wang S H, Lin L, Liu Y, Zhou Y S, Hu Y F and Wang Z L 2013 Theoretical study of contact-mode triboelectric nanogenerators as an effective power source *Energy Environ. Sci.* **6** 3576–83

[79] Kim J, Ryu H, Lee J H, Khan U, Kwak S S, Yoon H J and Kim S W 2020 High permittivity $CaCu_3Ti_4O_{12}$ particle-induced internal polarization amplification for high performance triboelectric nanogenerators *Adv. Energy Mater.* **10** 1903524

[80] Hu Y J, Wang Y L, Tian S D, Yu A F, Wan L Y and Zhai J Y 2021 Performance-enhanced and washable triboelectric air filter based on polyvinylidene fluoride/UiO-66 composite nanofiber membrane *Macromol. Mater. Eng.* **306** 2100128

[81] Hu X H, Bao X F, Zhang M M, Fang S L, Liu K Y, Wang J, Liu R M, Kim S H, Baughman R H and Ding J N 2023 Recent advances in carbon nanotube-based energy harvesting technologies *Adv. Mater.* **35** 2303035

[82] Shrestha K, Sharma S, Pradhan G B, Bhatta T, Maharjan P, Rana S M S, Lee S, Seonu S, Shin Y and Park J Y 2022 A siloxene/ecoflex nanocomposite-based triboelectric nanogenerator with enhanced charge retention by MoS_2/LIG for self-powered touchless sensor applications *Adv. Funct. Mater.* **32** 2113005

[83] Wang D Q, Ye J, Bai Y L, Yang F, Zhang J, Rao W and Liu J 2023 Liquid metal combinatorics toward materials discovery *Adv. Mater.* **35** 2303533

[84] Kim J, Lee J H, Ryu H, Lee J H, Khan U, Kim H, Kwak S S and Kim S W 2017 High-performance piezoelectric, pyroelectric, and triboelectric nanogenerators based on P(VDF-TrFE) with controlled crystallinity and dipole alignment *Adv. Funct. Mater.* **27** 1700702

[85] Song Z Q, Li W Y, Kong H J, Bao Y, Wang N, Wang W, Ma Y M, He Y, Gan S Y and Niu L 2022 Enhanced energy harvesting performance of triboelectric nanogenerator via efficient dielectric modulation dominated by interfacial interaction *Nano Energy* **92** 106759

[86] Jin L *et al* 2020 Manipulating relative permittivity for high-performance wearable triboelectric nanogenerators *Nano Lett.* **20** 6404–11

[87] Wang H L, Guo Z H, Zhu G, Pu X and Wang Z L 2021 Boosting the power and lowering the impedance of triboelectric nanogenerators through manipulating the permittivity for wearable energy harvesting *ACS Nano* **15** 7513–21

[88] Jiang F, Zhou X R, Lv J, Chen J, Chen J T, Kongcharoen H, Zhang Y H and Lee P S 2022 Stretchable, breathable, and stable lead-free perovskite/polymer nanofiber composite for hybrid triboelectric and piezoelectric energy harvesting *Adv. Mater.* **34** 2200042

[89] Wen R M, Guo J M, Yu A F, Zhai J Y and Wang Z L 2019 Humidity-resistive triboelectric nanogenerator fabricated

using metal organic framework composite *Adv. Funct. Mater.* **29** 1807655
[90] Cui N Y, Gu L, Lei Y M, Liu J M, Qin Y, Ma X H, Hao Y and Wang Z L 2016 Dynamic behavior of the triboelectric charges and structural optimization of the friction layer for a triboelectric nanogenerator *ACS Nano* **10** 6131–8
[91] Kim D W, Lee J H, You I, Kim J K and Jeong U 2018 Adding a stretchable deep-trap interlayer for high-performance stretchable triboelectric nanogenerators *Nano Energy* **50** 192–200
[92] Kim J K *et al* 2023 Electric-field-driven interfacial trapping of drifting triboelectric charges via contact electrification *Energy Environ. Sci.* **16** 598–609
[93] Chen X P, Liu Y N, Sun Y, Zhao T S, Zhao C, Khattab T A, Lim E G, Sun X H and Wen Z 2022 Electron trapping & blocking effect enabled by MXene/TiO_2 intermediate layer for charge regulation of triboelectric nanogenerators *Nano Energy* **98** 107236
[94] Huang T, Yu H, Wang H Z, Zhang Q H and Zhu M F 2016 Hydrophobic SiO_2 electret enhances the performance of poly(vinylidene fluoride) nanofiber-based triboelectric nanogenerator *J. Phys. Chem.* C **120** 26600–8
[95] Zhang X, Lv S S, Lu X C, Yu H, Huang T, Zhang Q H and Zhu M F 2020 Synergistic enhancement of coaxial nanofiber-based triboelectric nanogenerator through dielectric and dispersity modulation *Nano Energy* **75** 104894
[96] Tayyab M, Wang J, Wang J M, Maksutoglu M, Yu H D, Sun G Z, Yildiz F, Eginligil M and Huang W 2020 Enhanced output in polyvinylidene fluoride nanofibers based triboelectric nanogenerator by using printer ink as nano-fillers *Nano Energy* **77** 105178
[97] Rahman M T, Rana S M S, Zahed M A, Lee S, Yoon E S and Park J Y 2022 Metal-organic framework-derived nanoporous carbon incorporated nanofibers for high-performance triboelectric nanogenerators and self-powered sensors *Nano Energy* **94** 106921
[98] Zhang J H *et al* 2022 Coupling enhanced performance of triboelectric–piezoelectric hybrid nanogenerator based on nanoporous film of poly(vinylidene fluoride)/$BaTiO_3$ composite electrospun fibers *ACS Mater. Lett.* **4** 847–52
[99] Ippili S, Jella V, Thomas A M, Yoon C, Jung J S and Yoon S G 2021 ZnAl–LDH-induced electroactive β-phase and controlled dielectrics of PVDF for a high-performance triboelectric nanogenerator for humidity and pressure sensing applications *J. Mater. Chem.* A **9** 15993–6005
[100] Shi L *et al* 2021 High-performance triboelectric nanogenerator based on electrospun PVDF-graphene nanosheet composite nanofibers for energy harvesting *Nano Energy* **80** 105599
[101] Paranjape M V, Graham S A, Patnam H, Manchi P and Yu J S 2021 3D printed bidirectional rotatory hybrid nanogenerator for mechanical energy harvesting *Nano Energy* **88** 106250
[102] Zhang P, Zhang W K, Deng L and Zhang H H 2021 A triboelectric nanogenerator based on temperature-stable high dielectric $BaTiO_3$-based ceramic powder for energy harvesting *Nano Energy* **87** 106176
[103] Yang C R, Ko C T, Chang S F and Huang M J 2022 Study on fabric-based triboelectric nanogenerator using graphene oxide/porous PDMS as a compound friction layer *Nano Energy* **92** 106791
[104] Chen J, Guo H Y, He X M, Liu G L, Xi Y, Shi H F and Hu C G 2016 Enhancing performance of triboelectric nanogenerator by filling high dielectric nanoparticles into sponge PDMS film *ACS Appl. Mater. Interfaces* **8** 736–44
[105] Zhao X Y and Ounaies Z 2022 A facile method to enhance the flexibility and triboelectric output of PDMS using ionic liquid-coated single-wall carbon nanotubes *Nano Energy* **94** 106908
[106] Pang L L, Li Z K, Zhao Y L, Zhang X, Du W W, Chen L, Yu A F and Zhai J Y 2022 Triboelectric nanogenerator based on polyimide/boron nitride nanosheets/polyimide nanocomposite film with enhanced electrical performance *ACS Appl. Electron. Mater.* **4** 3027–35
[107] Wu C X, Kim T W, Park J H, An H Q, Shao J J, Chen X Y and Wang Z L 2017 Enhanced triboelectric nanogenerators based on MoS_2 monolayer nanocomposites acting as electron-acceptor layers *ACS Nano* **11** 8356–63
[108] Rana S M S, Zahed M A, Rahman M T, Salauddin M, Lee S H, Park C, Maharjan P, Bhatta T, Shrestha K and Park J Y 2021 Cobalt-nanoporous carbon functionalized nanocomposite-based triboelectric nanogenerator for contactless and sustainable self-powered sensor systems *Adv. Funct. Mater.* **31** 2105110
[109] Salauddin M *et al* 2022 Fabric-assisted MXene/silicone nanocomposite-based triboelectric nanogenerators for self-powered sensors and wearable electronics *Adv. Funct. Mater.* **32** 2107143
[110] Sha Z, Boyer C, Li G, Yu Y Y, Allioux F M, Kalantar-Zadeh K, Wang C H and Zhang J 2022 Electrospun liquid metal/PVDF-HFP nanofiber membranes with exceptional triboelectric performance *Nano Energy* **92** 106713
[111] Yu A F, Zhu Y X, Wang W and Zhai J Y 2019 Progress in triboelectric materials: toward high performance and widespread applications *Adv. Funct. Mater.* **29** 1900098
[112] Wang H M, Xu L, Bai Y and Wang Z L 2020 Pumping up the charge density of a triboelectric nanogenerator by charge-shuttling *Nat. Commun.* **11** 4203
[113] Bai Y, Xu L, Lin S Q, Luo J J, Qin H F, Han K and Wang Z L 2020 Charge pumping strategy for rotation and sliding type triboelectric nanogenerators *Adv. Energy Meter.* **10** 2000605
[114] Liu W L *et al* 2019 Integrated charge excitation triboelectric nanogenerator *Nat. Commun.* **10** 1426
[115] Liu Y K, Liu W L, Wang Z, He W C, Tang Q, Xi Y, Wang X, Guo H Y and Hu C G 2020 Quantifying contact status and the air-breakdown model of charge-excitation triboelectric nanogenerators to maximize charge density *Nat. Commun.* **11** 1599
[116] Lei R, Li S Y, Shi Y X, Yang P, Tao X L, Zhai H, Wang Z L and Chen X Y 2022 Largely enhanced output of the non-contact mode triboelectric nanogenerator via a charge excitation based on a high insulation strategy *Adv. Energy Mater.* **12** 2201708
[117] Guo Z T, Yang P Y, Zhao Z H, Gao Y K, Zhang J Y, Zhou L L, Wang J and Wang Z L 2023 Achieving a highly efficient triboelectric nanogenerator via a charge reversion process *Energy Environ. Sci.* **16** 5294–304
[118] Zhao Q H, Wu H Y, Wang J, Xu S Y, He W C, Shan C C, Fu S K, Li G, Li K X and Hu C G 2023 High-efficiency charge injection with discharge mitigation strategy for triboelectric dielectric materials *Adv. Energy Mater.* **13** 2302099
[119] Li Z K, Liu J T, Chi M S, Miao X, Yang H X, Cui W Q, Yu A F and Zhai J Y 2024 Ultra-high output triboelectric nanogenerator based on synergies of material modification and charge pumping *Chem. Eng. J.* **481** 148726
[120] Wu H Y, Wang J, He W C, Shan C C, Fu S K, Li G, Zhao Q H, Liu W L and Hu C G 2023 Ultrahigh output charge density achieved by charge trapping failure of dielectric polymers *Energy Environ. Sci.* **16** 2274–83
[121] Wang J, Zhang B F, Zhao Z H, Gao Y K, Liu D, Liu X R, Yang P Y, Guo Z T, Wang Z L and Wang J 2024 Boosting the charge density of triboelectric nanogenerator by

suppressing air breakdown and dielectric charge leakage *Adv. Energy Mater.* **14** 2303874
[122] Wang J, Wu H Y, Fu S K, Li G, Shan C C, He W C and Hu C G 2022 Enhancement of output charge density of TENG in high humidity by water molecules induced self-polarization effect on dielectric polymers *Nano Energy* **104** 107916
[123] Choi D *et al* 2023 Recent advances in triboelectric nanogenerators: from technological progress to commercial applications *ACS Nano* **17** 11087–219
[124] Pu J H *et al* 2023 Textile electronics for wearable applications *Int. J. Extrem. Manuf.* **5** 042007
[125] Wang J F, Suo J, Song Z X, Li W J and Wang Z B 2023 Nanomaterial-based flexible sensors for metaverse and virtual reality applications *Int. J. Extrem. Manuf.* **5** 032013
[126] Zhang C, Zhao J Q, Zhang Z, Bu T Z, Liu G X and Fu X P 2023 Tribotronics: an emerging field by coupling triboelectricity and semiconductors *Int. J. Extrem. Manuf.* **5** 042002